

Development of Next-Generation Optical Neural Silencers

by

Amy Chuong

B.S. in Biology - Cell, Developmental and Molecular Biology Track
Massachusetts Institute of Technology, 2009

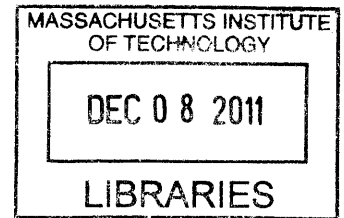
B.S. in Humanities and Science
Massachusetts Institute of Technology, 2009

Submitted to the Program in Media Arts and Sciences, School of Architecture and Planning,
in partial fulfillment of the requirements for the degree of
Master of Science in Media Arts and Sciences

at the

Massachusetts Institute of Technology

September 2011




ARCHIVES

© Massachusetts Institute of Technology 2011. All rights reserved.

Author: _____

Program in Media Arts and Sciences
School of Architecture and Planning
August 5, 2011

Certified by: _____



Edward S. Boyden, III, Ph.D.
Benesse Career Development Professor
Program in Media Arts and Sciences, MIT
Thesis Supervisor

Accepted by: _____

Mitchel Resnick, Ph.D.
LEGO Papert Professor of Learning Research
Academic Head
Program in Media Arts and Sciences

Development of Next-Generation Optical Neural Silencers

by

Amy Chuong

Submitted to the Program in Media Arts and Sciences,

School of Architecture and Planning,

on August 5, 2011

in partial fulfillment of the requirements for the degree of

Master of Science in Media Arts and Sciences

Abstract

The ability to rapidly and safely silence the electrical activity of individual neurons or neuron populations is invaluable in the study of brain circuit mapping. The expression of light-driven ion channels and pumps allows these pathways to be observed, mapped and controlled with millisecond timescale resolution. We here show that it is possible to mediate the powerful multiple-color silencing of neural activity through the heterologous expression of light-driven outward proton pumps and inward chloride pumps. We characterized a number of novel opsins through an exploration of ecological and genomic diversity, and further boosted opsin function and trafficking through the appendage of signal sequences. The green-light drivable archaerhodopsin-3 (Arch) from *Halorubrum sodomense* and the yellow-light drivable archaerhodopsin from *Halorubrum* strain TP009 (ArchT) are able to mediate complete neuron silencing in the *in vivo* awake mouse brain, and the blue-light drivable proton pump from *Leptosphaeria maculans* (Mac) opens up the potential for the multiple-color control of independent neuron populations. Finally, the principles outlined here can be extrapolated to the larger context of synthetic physiology.

Thesis Supervisor:

Edward S. Boyden, III

Benesse Career Development Professor

Program in Media Arts and Sciences

Reader: _____

Hugh Herr, Ph.D.

Associate Professor of Media Arts and Sciences

MIT Program in Media Arts and Sciences

Reader: _____

Chris A. Kaiser, Ph.D.

MacVicar Professor of Biology

Head of Department

MIT Department of Biology

Table of Contents

1. Introduction	6
1.1 Overview.....	6
1.2 Neuron electrophysiology	8
1.3 Microbial opsins	11
2. Mining Opsin Phylogenetic Diversity	13
2.1 Engineering Halo	13
2.2 Phylogenetic opsin screening.....	18
2.3 Arch implementation in the <i>in vivo</i> rodent brain	24
2.4 Multiple-color control of independent neuron populations	28
2.5 Discussion	30
3. ArchT: a novel, high-light sensitivity neural silencer	31
3.1 Engineering Arch	31
3.2 ArchT implementation in the <i>in vivo</i> rodent and primate brain	35
3.3 Discussion	39
4. Synthetic Physiology: Strategies for Adapting Tools From Nature	40
4.1 Molecular design and construction.....	40
4.2 Transduction of microbial opsins into cells for heterologous expression.....	44
4.3 Physiological assays.....	48
4.4 Conclusion	52
5. Summary and Further Work	53
6. Experimental Methods	54
6.1 Plasmid construction and site directed mutagenesis.....	54
6.2 Neuron culture, transfection, infection, and imaging	56
6.3 HEK 293FT cell culture and transfection	57
6.4 Lentivirus preparation.....	57
6.5 Virus injection in the adult mouse.	58
6.6 <i>In vitro</i> whole cell patch clamp recording & optical stimulation	58
6.7 <i>In vivo</i> rodent electrophysiology, optical stimulation, and data analysis.	60
6.8 <i>In vivo</i> primate electrophysiology, optical stimulation, and data analysis.....	61
6.9 Histology	63
7. Acknowledgements	64
8. References	65

1. Introduction

1.1 Overview

A fundamental challenge in biology is the spatiotemporally precise study and control of complex systems. Classical methods such as physical ablation, electrode stimulation, and genetic knockout are crude and invasive, while exogenous ligand addition and drug delivery are spatially imprecise due to their diffusible natures. Optogenetics, which combines molecular biology -- in the form of genetically engineering light-drivable proteins -- and optical stimulation from sophisticated light-delivery hardware offers a tantalizing alternative. The heterologous expression of light-drivable ion channels and pumps such as the depolarizing channelrhodopsin-2 (ChR2)¹ from the algae *Chlamydomonas reinhardtii* and the hyperpolarizing halorhodopsin (halo/NpHR)^{2,3} from the halobacterium *Natromonas pharaonis* allows neural circuits to be observed, mapped, and controlled with great spatial precision and millisecond timescale resolution.

Although optogenetics is a young field, its scope has rapidly expanded in the past half-decade. The ability to precisely control neural circuits has proven invaluable in understanding complex brain modalities such as aggression⁴, anxiety⁵, autism⁶ and drug abuse⁷, and physiological processes such as cardiac arrhythmia⁸ and muscle fiber contractions⁹. Yet there is still much room for improvement. The high-level, heterologous expression of these proteins in the mammalian brain may lead to intracellular aggregates and possible toxicity, as well as a significantly lower yield of functional protein. Improving opsin kinetics would extend the length of time that neuronal populations can be silenced, as well as enabling the creation of sustained, high-frequency neuron spike trains. Low light sensitivity is critical to the silencing of larger brain regions, which in turn reduces the invasiveness of surgically implanted optical hardware. Finally, creating opsins which are responsive to different light wavelengths enables the creation of a spectral toolbox of optical sensitizers, and the multiple color control of independent neuron populations.

This thesis presents three novel optical silencers identified through an exploratory screen of ecological and genomic diversity, and discusses the underlying biological principles. Section 1.1 introduces the importance of optical neural control as well as some major goals and considerations of opsin engineering. Section 1.2 describes neuron electrophysiology and the electrophysiological techniques involved in optogenetics. Section 1.3 discusses the larger microbial rhodopsin families in the context of member diversity and protein structure.

Chapter 2 presents two novel optogenetic silencers, known as Arch and Mac, which function as proton pumps rather than chloride pumps. Chapter 3 presents ArchT, an improved version of Arch which was identified through a directed genomic screen for Arch relatives. Chapter 4 discusses some of the principles involved in developing novel optogenetic tools and the ways in which they can be extrapolated to the larger field of synthetic physiology. Chapter 5 presents the experimental methods. Finally, chapter 6 summarizes the presented work and proposes future directions of study.

1.2 Neuron electrophysiology

Action potential shape and kinetics in the brain are very cell-type dependent, but some generalizations can be made for all neurons. In its resting state, a neuron has a voltage difference of approximately -60 mV across the cell plasma membrane (Figure 1-1) which is referred to as the resting potential (V_{rest}). This voltage difference is established by ion pumps and channels which maintain a not-insignificant number of ion concentration gradients (Table 1).

Ion	Intracellular range (mM)	Extracellular range (mM)
Na ⁺	5-20	130-160
K ⁺	130-160	4-8
Ca ²⁺	0.05-1.0	1.2-4
Mg ²⁺	10-20	1-5
Cl ⁻	1-60	100-140
HCO ³⁻	1-3	20-30

Table 1.1 | Intracellular and extracellular distribution of the main ions found in animal fluids. (Figure adapted from Molleman 2003¹⁰)

The tendency of ions to move with the concentration gradient, or from a region of higher concentration to lower concentration, can be mathematically described as:

$$\Delta G = -RT \ln \frac{[\text{ion}]_{\text{extracellular}}}{[\text{ion}]_{\text{intracellular}}}$$

where ΔG is the Gibbs energy released by diffusion, R is the universal gas constant ($-8.31 \text{ J mol}^{-1} \text{ K}^{-1}$), T is temperature in degrees Kelvin, and $[\text{ion}]_{\text{extracellular}}$ and $[\text{ion}]_{\text{intracellular}}$ refer to the respective extracellular and intracellular concentrations of the given ion.

Action potentials are initiated with the depolarization of a small patch of cell membrane, which

allows that region to reach a voltage threshold of approximately -50 mV (**Figure 1-2**). This voltage deflection causes additional sodium channels to open. Sodium ions rapidly enter the cell in accordance with the sodium ion concentration gradient, and the rapid influx of positive charge causes the neuron to rapidly depolarize to 0 mV, then overshoot to a level of approximately +50 mV (**Figure 1-3**). Subsequently, the sodium channel gates close, and voltage-gated potassium channels open (**Figure 1-4**). The cell then repolarizes, voltage briefly falling below the normal resting potential (afterhyperpolarization) (**Figure 1-5**), before returning to its initial -60 mV resting state (**Figure 1-6**).

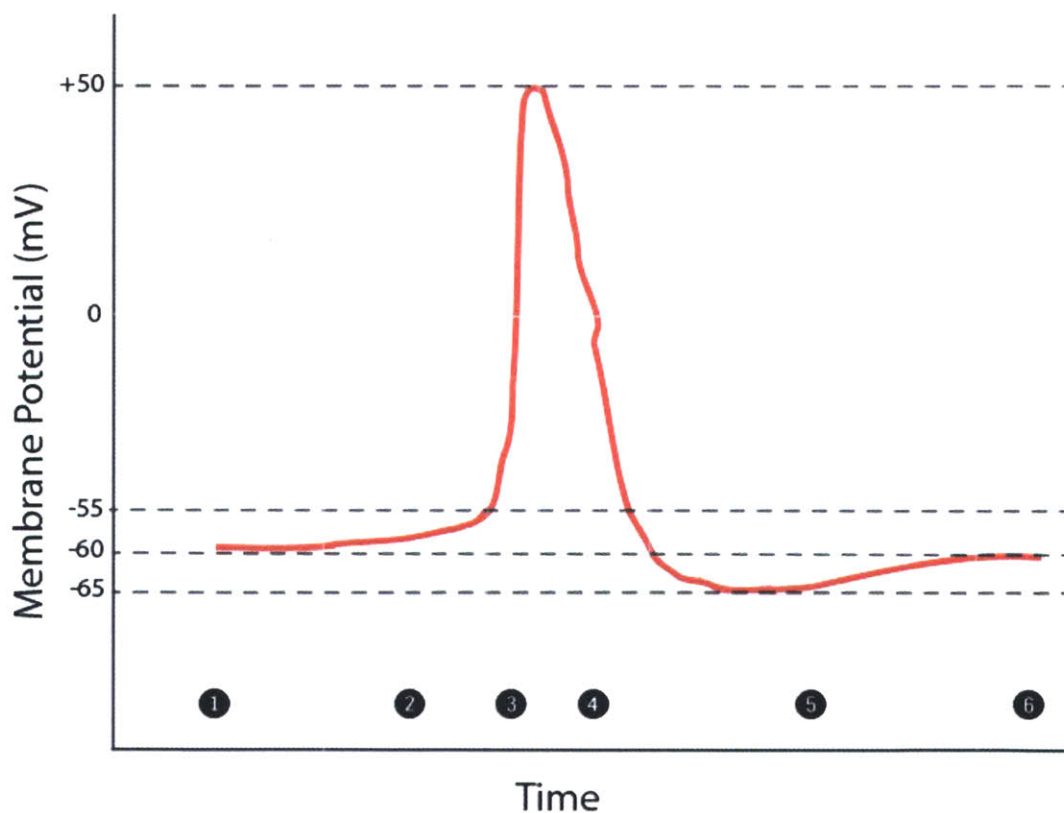


Figure 1 | A Neuron Action Potential. (1) Neuron in its resting state. (2) Action potential initiation, cell begins to approach voltage threshold. (3) Rapid depolarization. (4) Voltage gated potassium channels open, causing repolarization. (5) Afterhyperpolarization. (6) Return to resting state.

Neuron voltage deflections and the corresponding action potentials (or lack thereof) are assessed

in this thesis by one of two means: whole-cell patch clamp and extracellular recording.

Whole-cell patch clamping was developed by Erwin Neher and Bert Sakmarr in the late 1970s¹¹, who later won the Nobel Prize in Physiology or Medicine in 1991 for their work. A glass micropipette with an open tip diameter of 1-2 μm is used to approach the cell under study, and suction is used to first create a high resistance gigaohm seal between the glass and cell membrane, then to rupture the region of cell membrane directly in contact with the glass micropipette opening. The glass micropipette subsequently has access to the cell cytoplasmic space and is referred to as the intracellular electrode. Another electrode is placed in the bath solution to serve as a ground. Recordings are then taken either in voltage-clamped mode (measuring the amount of current which must be injected in order to maintain a constant voltage difference across the cell membrane), or in current-clamped mode (which maintains a constant amount of injected current while measuring voltage deflections). Both voltage- and current-clamped recordings are standard practice within optogenetics, but this thesis primarily uses voltage-clamped recordings to assess photocurrent. Photocurrent is here defined as the amount of charge generated by ion influx or efflux within the cell as a result of optical stimulation.

In contrast to whole-cell patch clamp, extracellular recording measures extracellular matrix voltage deflections generated by the current fields outside the neuron as a result of action potentials. The activity of one or multiple neurons may be recorded, depending on electrode tip size and local neuron density, and referred to respectively as "single-unit" or "multi-unit" recordings. While the obtained data has a significantly smaller signal than whole-cell patch clamp, extracellular recording can be conducted *in vivo* on awake, restrained animals. Further, extracellular recordings can be used to simultaneously determine the signaling state of a neuron population, rather than that of individual cells, and recordings can be carried out for much longer time durations without the time limits cell dialysis imposes on whole-cell patch clamp.

1.3 Microbial opsins

While all members of the opsin superfamily share a highly characteristic seven transmembrane alpha-helical structure and retinal chromophore attached to a conserved lysine residue (Figure 2), primary sequence alignments divide them into two independent protein families: the type 1 opsins which play a role in phototaxis and light-driven ion transport in both eukaryotic and prokaryotic microbial species, and the type 2 opsins, which mediate vision and circadian rhythms in higher eukaryotes. At present, it is unknown whether the two families descend from a single progenitor ancestor or whether they are the product of convergent evolution¹². The presence of type 1 opsins among organisms as diverse as archaea, bacteria, and fungi may either be the result of a shared common ancestor, or horizontal gene transfer within the haloarchaea¹³.

Functionally, type 1 microbial opsins can be divided into transporters and receptors.

Bacteriorhodopsin, one of the most extensively studied of all opsins, was identified by Oesterhelt and Stoeckenius in 1971¹⁴ from the archaeal *Halobacterium halobium* and soon determined to be a light-dependent proton pump¹⁵. Subsequent work was carried out in *Halobacterium* to identify similar light-sensitive proteins and halorhodopsin^{16,17,18}, sensory rhodopsin I^{19,20,21,22} and sensory rhodopsin II^{23,24,25,26,27,28} (also known as phoborhodopsin) were isolated and characterized over the next two decades. Of these, bacteriorhodopsin and halorhodopsin are transporters -- ion pumps which respectively generate proton electrochemical potentials for ATP production and hyperpolarize the cell membrane via chloride transport -- and the sensory rhodopsins serve as "visual" photoreceptors for microbial phototaxis in low oxygen environments.

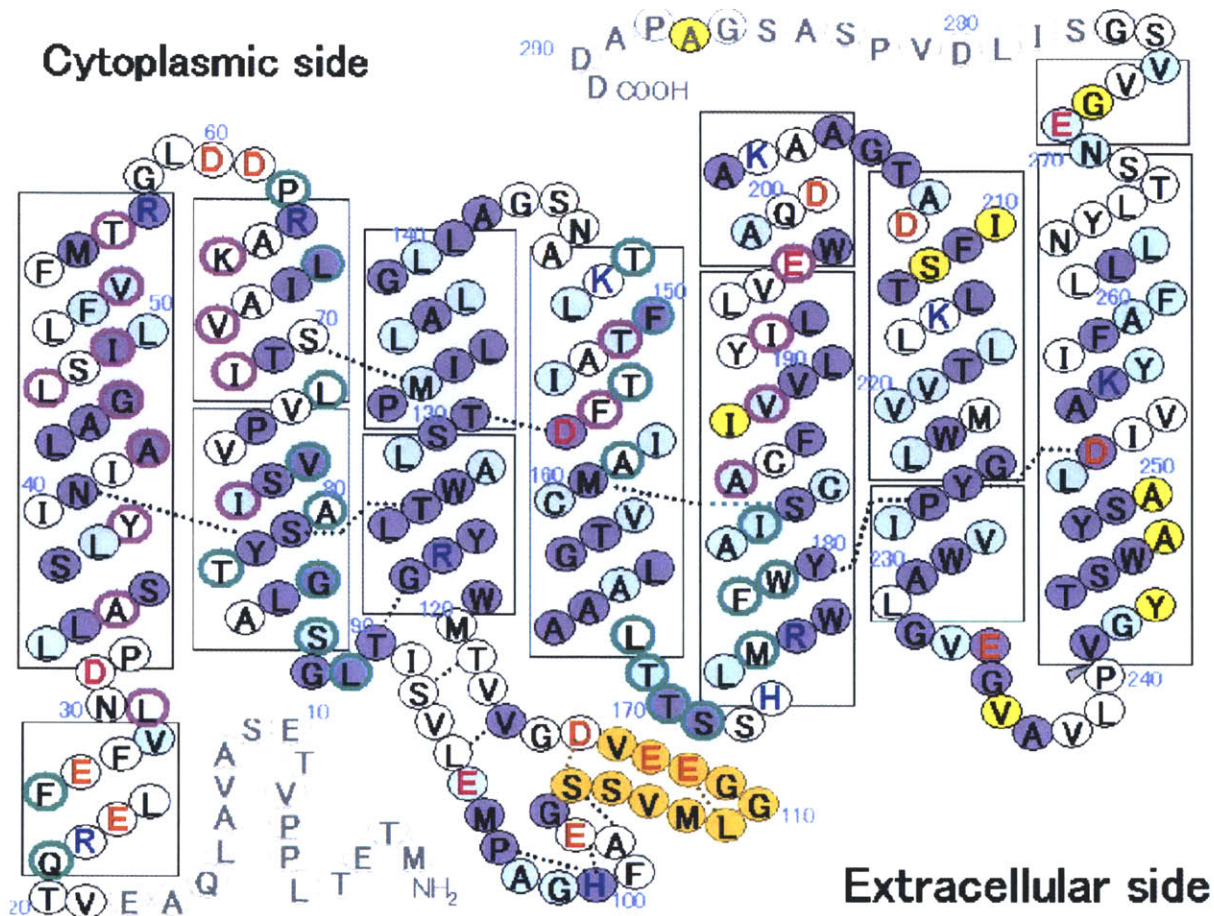


Figure 2 | *Natromonas pharaonis* halorhodopsin structure. Schematic of the classic seven-transmembrane helix opsin structure. (Figure adapted from Kouyama *et al.* 2010²⁹)

Extensive structural work has been conducted on the type 1 microbial opsins. Electron crystallographic analyses of bacteriorhodopsin were carried out by Henderson and Unwin to a resolution of 7 Å as early as 1975³⁰. This work was later improved on, yielding a number of electron and x-ray crystallography structures^{31,32,33,34,35}, culminating in the 1.6 Å structure reported by Luecke and colleagues in 1999³⁶. High resolution structures of halorhodopsin have also been obtained for the *Halobacterium salinarum* strain in 2000^{37,38} and for the *Natromonas pharaonis* strain in 2010²⁹. Finally, sensory rhodopsin II has additionally been crystallized³⁹. Remarkably, the helix architecture is highly conserved among all four types of type 1 microbial opsins from the same organism, and additionally within orthologs, suggesting a potential underlying architecture that can be engineered across all microbial opsins.

2. Mining Opsin Phylogenetic Diversity

The work outlined in this chapter resulted in the publication of “High-performance genetically targetable optical neural silencing by light-driven proton pumps” in *Nature* (2010) by Brian Chow and colleagues⁴⁰. My contribution to this project was in the area of gene cloning, virus making, and cell culture transfection.

2.1 Engineering Halo

The heterologous expression of the *Natromonas pharaonis* halorhodopsin (halo/NpHR) in neurons^{2,3} to achieve light-drivable silencing represented a major stride forward for the burgeoning field of optogenetics. A hyperpolarizing complement to the depolarizing ChR2 now existed for the first time, allowing the transient silencing of neuron populations and enabling bidirectional signaling within the same cell (**Figure 2**).

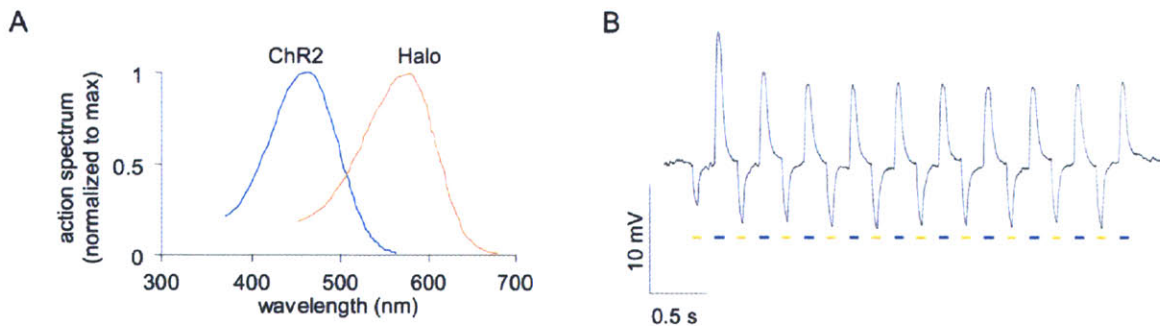


Figure 3 | Single-cell bidirectional signaling using stoichiometric co-expression of Halo and ChR2. (A) Overlaid peak-normalized action spectra for ChR2 and Halo. **(B)** Hyperpolarization and depolarization events elicited in a single representative neuron by blue and yellow light pulse trains. (Figure adapted from Han *et al.* 2009⁴¹)

Yet despite its great *in vitro* promise, Halo still has a number of problems which needed to be solved for *in vivo* implementation. When expressed at high levels, such as those seen with high titer virus or in transgenic mice, Halo forms puncta and intracellular blebs (Figure 4).

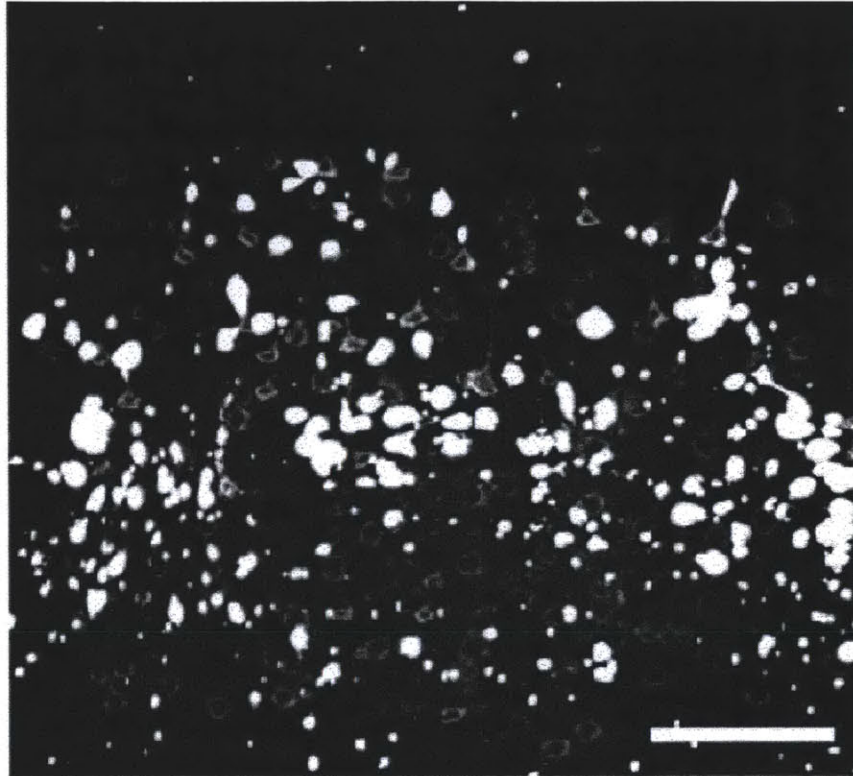


Figure 4 | Poor membrane expression and intracellular blebbing in Halo transgenic mice. NpHR-YFP forms numerous intracellular blebs in neurons of Thy1-NpHR-YFP transgenic mice. Scale bars: 100 μm . (Figure adapted from Zhao *et al.* 2008⁴¹)

Additionally, Halo's pumping activity -- and with it, its ability to silence neurons -- runs down and the protein inactivates during long periods of illumination (**Figure 5**). While this phenomenon can be addressed via blue-light resets, there are many situations in which it may not be experimentally desirable to have two optics sources. Additionally, it would be advantageous to boost the single-molecule efficacy of Halo, as this would enable the more powerful silencing of individual neurons, and additionally the silencing of much larger brain regions.

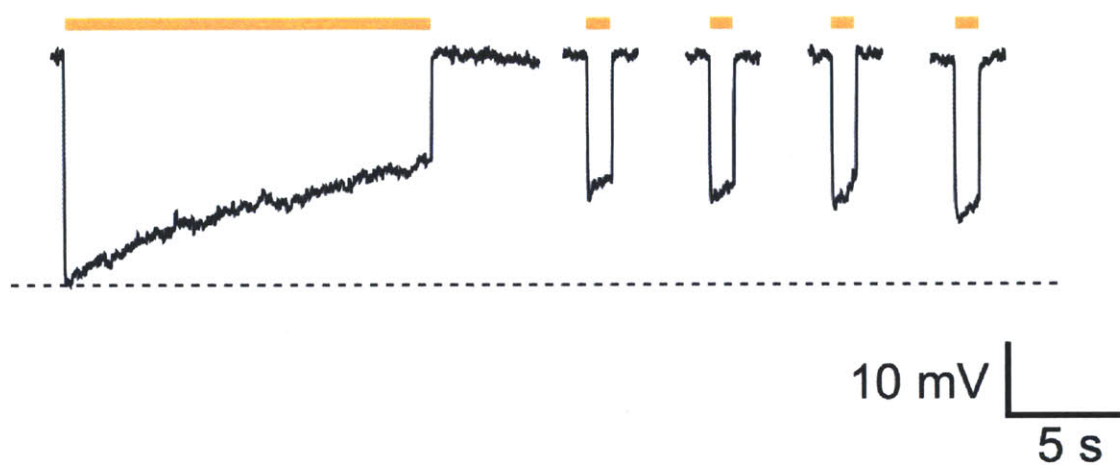


Figure 5 | Halo inactivation during sustained periods of illumination. Time-course of Halo-mediated hyperpolarizations in a representative current-clamped hippocampal neuron during 15 seconds of continuous yellow light, followed by four 1 second test pulses of yellow light (one every 30 seconds, starting 10 seconds after the end of the first 15-second period of yellow light. (Figure adapted from Han & Boyden 2007²)

In order to improve upon Halo, we screened a number of trafficking sequences and point mutants in HEK 293FT cells to see if it was possible to achieve spectral shift or to generate a Halo mutant which could spontaneously recover its active pumping state in the dark over a second timescale without blue-light illumination (**Table 2**). 'Recovery' residues were targeted based on hypothesized roles in chloride affinities and/or transport kinetics, as determined by structure-function studies and mutagenesis studies using other halorhodopsins^{42,43,44,45}. Spectral residues were targeted based upon their predicted retinal flanking locations based on crystal structures, and/or have been previously shown to govern the bacteriorhodopsin spectrum^{37,46,47,48,49,50}.

Halo point mutant	Homologous <i>H. salinarum</i> HR residue	Homologous <i>H. salinarum</i> BR residue	Primary predicted outcome of mutation	Primary Peak \pm FWHM (nm), second order Gaussian fit	Recovery of active pumping in dark?
Wild type	N/A	N/A	N/A	584 \pm 51	No
T126H	T111	D85	Recovery	No measured photocurrent	No
T126R	T111	D85	Recovery	No measured photocurrent	No
W127F	W112	W86	Spectral shift	No measured photocurrent	No
S130T	S130	T89	Recovery	568 \pm 55	No
S130D	S130	T89	Recovery	No measured photocurrent	No
S130H	S130	T89	Recovery	No measured photocurrent	No
S130R	S130	T89	Recovery	No measured photocurrent	No
A137T	A122	D96	Recovery	585 \pm 52	No
A137D	A122	D96	Recovery	575 \pm 53	No
A137H	A122	D96	Recovery	No measured photocurrent	No
A137R	A122	D96	Recovery	No measured photocurrent	No
G163C	G148	G122	Spectral shift	No measured photocurrent	No
W179F	W164	W137	Spectral shift	No measured photocurrent	No
S183C	F168	S141	Spectral shift	No measured photocurrent	No
F187M	F172	M145	Spectral shift	589 \pm 52	No
F187A	F172	M145	Spectral shift	No measured photocurrent	No
K215H	R200	R149	Recovery	586 \pm 50	No
K215R	R200	R149	Recovery	575 \pm 51	No
K215Q	R200	R149	Recovery	585 \pm 56	No
T218S	T203	T178	Recovery	582 \pm 53	No
T218D	T203	T178	Recovery	No measured photocurrent	No
T218H	T203	T178	Recovery	No measured photocurrent	No

Halo point mutant	Homologous <i>H. salinarum</i> HR residue	Homologous <i>H. salinarum</i> BR residue	Primary predicted outcome of mutation	Primary Peak \pm FWHM (nm), second order Gaussian fit	Recovery of active pumping in dark?
T218R	T203	T178	Recovery	No measured photocurrent	No
W222F	W207	W182	Spectral shift	No measured photocurrent	No
P226V	P211	P186	Spectral shift	No measured photocurrent	No
P226G	P211	P186	Spectral shift	No measured photocurrent	No
W229F	W214	W189	Spectral shift	587 \pm 53	No

Table 2 | Action spectrum and spontaneous recovery to active pumping state in the dark for *N. pharaonis* halorhodopsin point mutants examined in HEK293FT cells. (Table adapted from Chow *et al.* 2010⁵¹)

We additionally screened a number of signal sequences from the MHC Class I antigen ('ss')⁵², prolactin ('prl')⁵³, and an ER export sequence from the potassium channel Kir2.1 ('ER2')^{41,54} to see if it was possible to improve Halo photocurrents and trafficking. While photocurrents did improve relative to the wildtype, presumably through improving functional protein yield, we did not observe changes in Halo spectral shift or photorecovery (data not shown).

For these reasons, we thought it would be advantageous to mine genomic diversity to see whether other opsins existed which naturally possessed the properties of interest.

2.2 Phylogenetic opsin screening

We screened a total of seventeen type I microbial opsins (Table 3) from archaeobacteria, bacteria, plants, and fungi to identify light-driven hyperpolarizers which had improved photocurrents and action spectra. Mammalian codon-optimized genes were synthesized, cloned into GFP-fusion expression vectors under the CamKII promoter, and transfected into primary hippocampal or cortical neuron cultures. Opsin photocurrents were measured via whole-cell patch clamp, and additionally reported as photocurrent densities by normalizing for cell-capacitance as a measure of cell size, and spectrum normalized photocurrent densities by adjusting for different opsin spectral peaks (Figure 6).

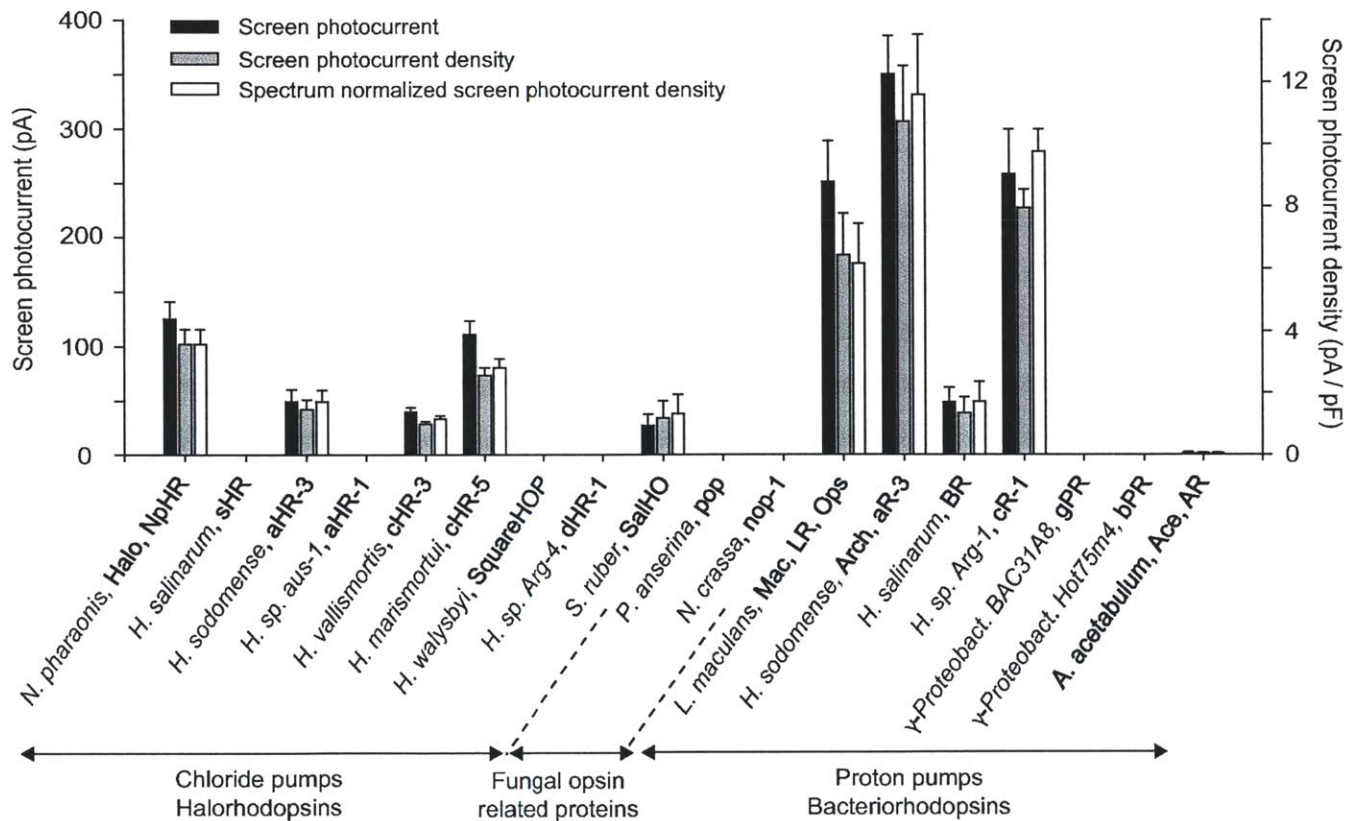


Figure 6 | Cross-kingdom photocurrent screen of optical neural silencers.

Screen data showing outward photocurrents (left y axis, black bars), photocurrent densities (right y axis, grey bars), and action spectrum-normalized photocurrent densities (right y axis, white bars), measured by whole-cell patch-clamp of

cultured neurons under screening illumination conditions (575 ± 25 nm, 7.8 mW/mm² for all except Mac/LR/Ops, gPR, bPR and Ace/AR, which were 535 ± 25 nm, 9.4 mW/mm²; n=4–16 neurons for each bar). Data are mean and s.e. Full species names from left to right: *Natronomonas pharaonis*^{2,3,55}, *Halobacterium salinarum*^{55,56}, *Halorubrum sodomense*⁵⁶, *Halorubrum species aus-1*⁵⁶⁻⁵⁷, *Haloarcula vallismortis*^{58,59}, *Haloarcula marismortui*^{59,60}, *Haloquadratum walsbyi*⁶¹, *Haloterrigena species Arg-4*^{56,59}, *Salinibacter ruber*^{62,63}, *Podospora anserina*⁶⁴, *Neurospora crassa*⁶⁵, *Leptosphaeria maculans*⁶⁶, *Halorubrum sodomense*⁵⁶, *Halobacterium salinarum*^{55,56}, *Haloarcula species Arg-1*⁶⁷, *uncultured gamma-proteobacterium BAC31A8*^{68,69}, *uncultured gamma-proteobacterium Hot75m4*^{68,69} and *Acetabularia acetabulum*⁷⁰. (Figure adapted from Chow & Han *et al.* 2010⁵¹)

Abbreviations	Molecule class	Species of origin	GENBANK Accession	References
Halo, NpHR, pHR	halorhodopsin	<i>Natronomonas pharaonis</i>	ABQ08589	2,3,55
sHR, HR	halorhodopsin	<i>Halobacterium salinarum</i>	NP_279315	55,56
aHR-3	archaealorhodopsin	<i>Halorubrum sodomense</i>	BAA75202	56
aHR-1, SGHR	archaealorhodopsin	<i>Halorubrum aus-1</i> (<i>sp. SG1</i>)	CAA49773	56-57
cHR-3	cruxhalorhodopsin	<i>Haloarcula vallismortis</i>	BAA06679	58,59
cHR-5	cruxhalorhodopsin	<i>Haloarcula marismortui</i>	AAV46572	59,60
SquareHOP	square halorhodopsin	<i>Haloquadratum walsbyi</i>	CAJ53165	61

dHR-1	deltahalorhodopsin	<i>Haloterrigena sp.</i> <i>Arg-4</i>	BAA75201	56,59
SalHO, SRU_2780	bacterial halorhodopsin	<i>Salinibacter ruber</i>	AAT76430	62,63
pop	fungal opsin related protein	<i>Podospora</i> <i>anserina (DSM980)</i>	XP_0019042 82	64
nop-1	fungal opsin related protein	<i>Neospora crassa</i>	XP_959421	65
Mac, LR, Ops	Fungal opsin related protein, bacteriorhodopsin	<i>Leptosphaeria</i> <i>maculans</i>	AAG01180	66
Arch, aR-3	archaerhodopsin	<i>Halorubrum</i> <i>sodomense</i>	BAA09452	56
BR	Bacteriorhodopsin	<i>Halobacterium</i> <i>salinarum</i>	CAA23744	56
cR-1	Cruxrhodopsin	<i>Haloarcula</i> <i>argentinensis (sp.</i> <i>arg-1</i>	BAA06678	67
gPR, BAC31A8	Proteorhodopsin	<i>γ-proteobacterium</i> <i>BAC31A8</i>	AAG10475	68,69
bPR, Hot75m4	proteorhodopsin	<i>γ-proteobacterium</i> <i>Hot75m4</i>	Q9AFF7	68,69
Ace, AR	Algal bacteriorhodopsin	<i>Acetabularia</i> <i>acetabulum</i>	AAY82897	70

Table 3 | Summary of molecular screening candidates, including abbreviations, molecule classification, species of origin, GenBank accession number, and references.

Of these constructs, the putative proton pump archaerhodopsin-3 from *H. sodomense* (Arch/aR-3)⁷¹ generated the highest photocurrents. Two other proton pumps, the *Leptosphaeria maculans* opsin (Mac/LR/Ops)⁶⁶ and cruxrhodopsin-1⁶⁷

also had significantly larger photocurrents than the *Natromonas pharaonis* halorhodopsin. All of the assessed light-driven proton pumps had higher screen photocurrents than the light-driven proton pumps.

We assessed Arch and Halo membrane expression using confocal microscopy and found that Halo and Arch possessed similar absolute expression levels on the cell plasma membrane⁵¹. Unlike Halo, Arch traffics well to the cell membrane without signs of intracellular aggregates (**Figure 7**).

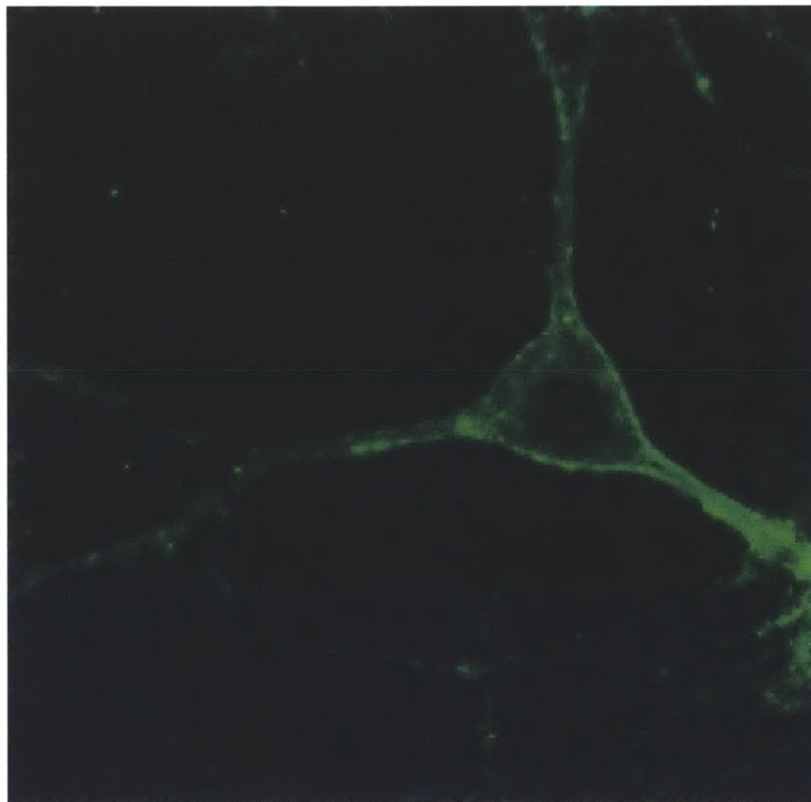


Figure 7 | Confocal fluorescence image of a lentivirally infected cultured neuron expressing Arch-GFP under the CamKII promoter.

Arch-mediated currents exhibited excellent kinetics of light-activation (8.8 ± 1.8 ms, $n=16$) and post-light-recovery (19.3 ± 2.9 ms, $n=16$). Unlike the wildtype Halo and Halo mutants, Arch spontaneously recovered light function within a timescale of seconds (**Figure 8**), and

demonstrated a significant dynamic range. At low light irradiances of 0.35 and 1.28 mW/mm² (**Figure 9i**), neural currents were 120 and 189 pA, respectively; at higher light powers (at which Halo currents saturate), Arch currents continued to increase, approaching 900 pA at effective irradiances of 36 mW/mm² (**Figure 9ii**).

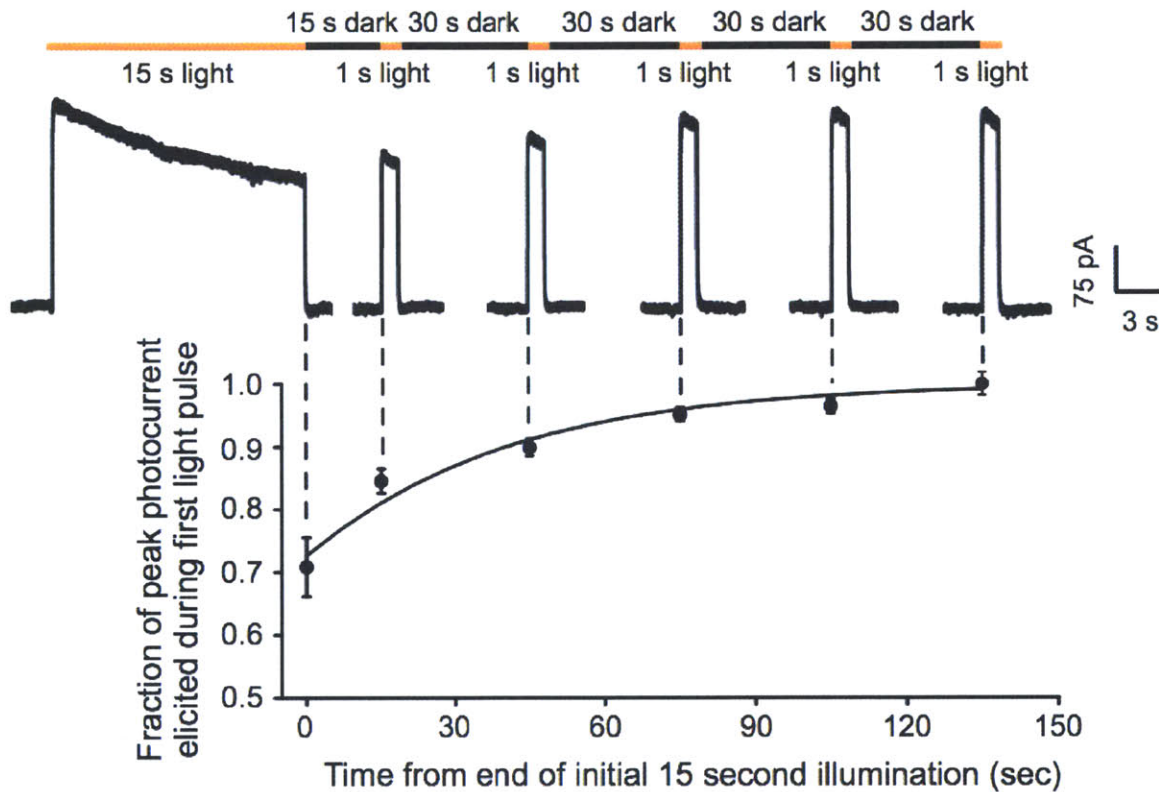


Figure 8 | Arch spontaneously recovers pumping post-illumination. Top half shows raw current trace of a neuron lentivirally infected with Arch, illuminated by a 15-s light pulse (575 ± 25 nm, 7.8 mW/mm²) followed by 1-s test pulses delivered at 15, 45, 75, 105 and 135 s after the end of the 15-s light pulse. Bottom half of graph shows population data of averaged Arch photocurrents (n=11 neurons) sampled at the times indicated by the vertical dotted lines.

(Figure adapted from Chow & Han *et al.* 2010⁵¹)

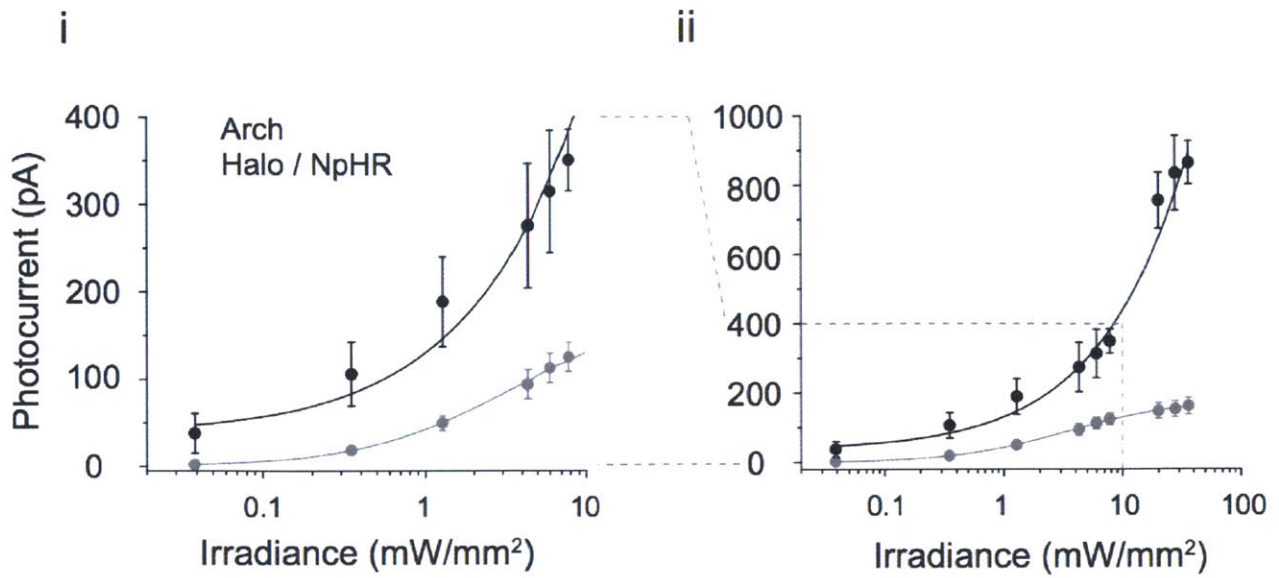


Figure 9 | Arch has significantly greater dynamic range than Halo.

Photocurrents of Arch versus Halo measured as a function of 575 ± 25 nm light irradiance in patch-clamped cultured neurons ($n = 4-16$ neurons for each point), for low (left) and high (right) light powers. The line is a single Hill fit to the data. (Figure adapted from Chow *et al.* 2010⁵¹)

2.3 Arch implementation in the *in vivo* rodent brain

We first estimated the tissue volumes which could be silenced, using *in vitro* culture data to estimate photocurrents for different irradiances and computational Monte Carlo simulations (Figure 10). We chose 0.35, 1.28, and 6 mW/mm² in order to simulate irradiance at 1.7, 1.2, or 0.6 mm away from the tip of a 200 μm fiber emitting 200 mW/mm², and measured the reduction in spike rate for each condition. Arch expressing neurons were significantly more inhibited than eNpHR-expressing cells, suggesting a 10-fold increase in brain tissue volume that would be ~50% silenced.

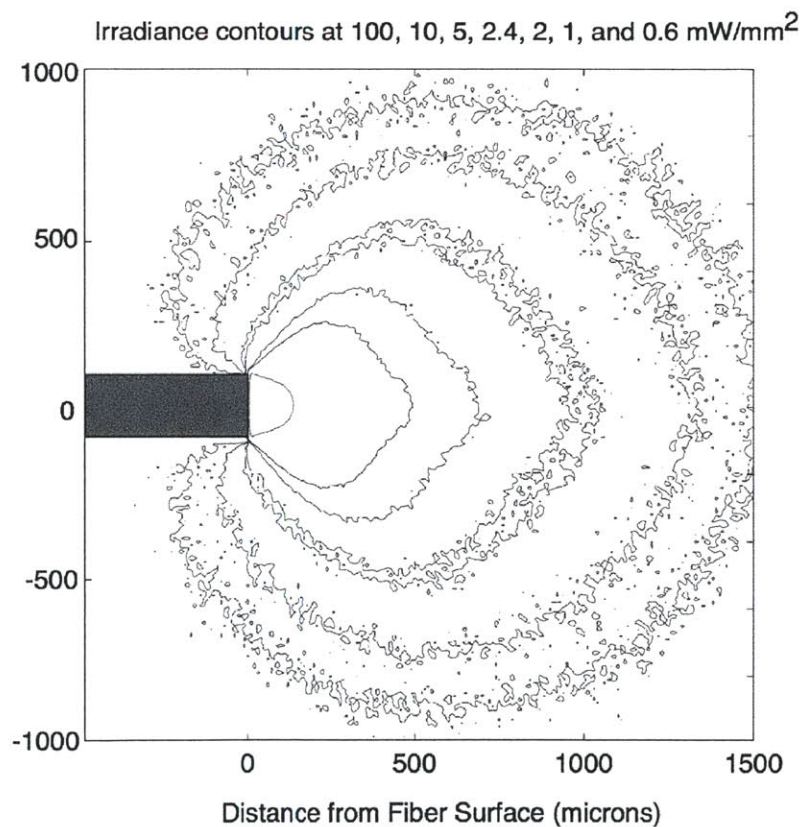


Figure 10 | Irradiance contours for 593 nm yellow light in the brain. 593 nm light is plotted as a function of location with respect to the top of a 200 μm fiber emitting 200 mW/mm² at the fiber tip into gray matter. Light irradiance was estimated using a Monte Carlo light scattering/absorption simulation. (Figure

adapted from Chow *et al.* 2010⁵¹)

To directly assess Arch's behavior *in vivo*, we injected encoding for Arch under the CamKII promoter into the mouse cortex and recorded neural responses ~1 month later via extracellular recording. We recorded neurons in awake head-fixed mice, illuminating neurons with a 200- μm optical fiber coupled to a 593 nm laser. The firing rate of many neurons immediately and strongly declined after light onset, and remained low throughout the illumination duration for both brief (**Figure 11a**, top) and long durations (**Figure 11a**, bottom).

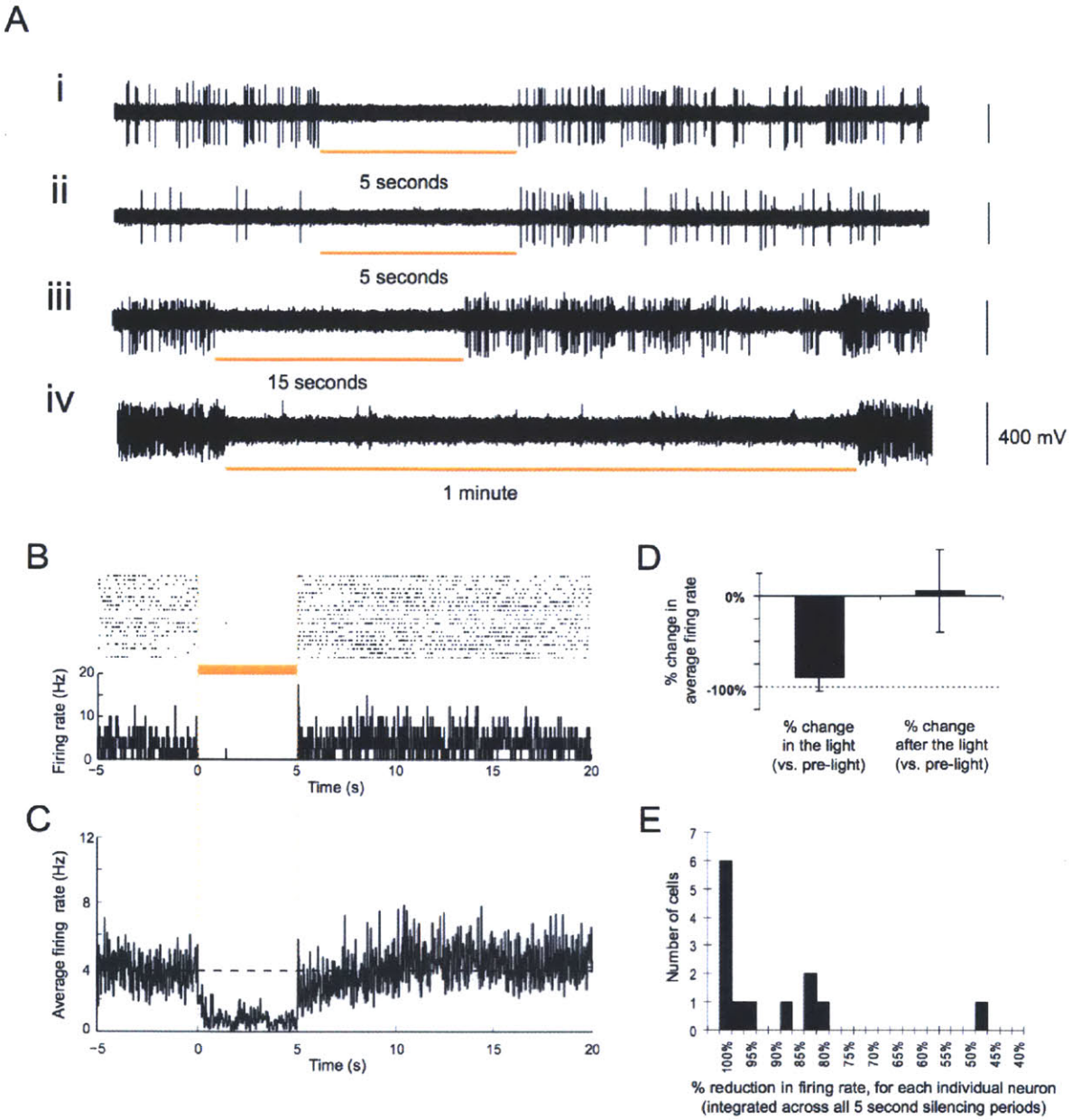


Figure 11 | High-performance Arch-mediated optical neural silencing of neocortical regions in awake mice. (A) Representative extracellular recordings showing neurons undergoing 5-s, 15-s, and 1-min periods of light illumination. (B) Neural activity in a representative neuron before, during, and after 5 s of yellow light illumination, shown as a spike raster plot (top) and as a histogram of instantaneous firing rate averaged across trials (bottom; bin size, 20 ms). (C) Population average of instantaneous firing rate before, during and after yellow

light illumination (black line, mean; gray lines, mean \pm s.e.; n = 13 units). (D) Average change in spike firing during 5-s of yellow light illumination (left) and during the 5 s immediately after light offset (right), for the data shown in B. (E) Histogram of percentage reductions in spike rate, for each individual neuron, integrated across all 5-s silencing periods.

We recorded 13 single-units that showed any decrease in firing during illumination and found spiking rates during exposure to 5 seconds of yellow light (Figure 11b) to drop by an average of $90 \pm 15\%$ (mean \pm s.d.; Figure 11c, d) and restoring to levels indistinguishable from the baseline after light cessation ($P > 0.2$, paired t-test; Figure 11d). Six of the 13 units decreased spike rate by at least 99.5%, and the median decrease was 97.1% (Figure 11e). One possibility is that Arch-expressing cells were almost completely silenced, whereas non-infected cells also decreased activity owing to network activity reduction during illumination.

The kinetics of silencing were rapid: for the six neurons that underwent $>99.5\%$ silencing, spike firing reduced with near-0-ms latency, rarely firing spikes after light onset; averaged across all cells, firing-rate reductions plateaued within 229 ± 310 ms (mean \pm s.d.) after light onset. After light cessation, the initial firing rate rapidly restored itself for the highly silenced neurons; averaged across all cells, firing rates took 355 ± 505 ms to recover after light offset. The level of post-light firing did not vary with repeated light exposure. Thus, Arch can mediate reliable silencing of neurons in the awake mammalian brain.

2.4 Multiple-color control of independent neuron populations

Great spectral diversity can be found in the proton pumps, in contrast to chloride pumps, which are primarily driven by yellow-orange light. The light-driven proton pump Mac in our screen had an action spectrum strongly blue-shifted relative to the light-driven chloride pump Halo (**Figure 12a**). We found that Mac-expressing neurons undergo four-fold larger hyperpolarizations with blue light than with red light, while Halo-expressing neurons undergo three-fold larger hyperpolarizations with red light than with blue (**Figure 12b**). Accordingly, we were able to demonstrate selective neural silencing in Mac-expressing neurons in response to blue light, and selective silencing of spike-firing in Halo-expressing neurons in response to red light (**Figure 12c**). It is clear that the spectral diversity of proton pumps enables the possibility of independent multicolor silencing of separate neural populations.

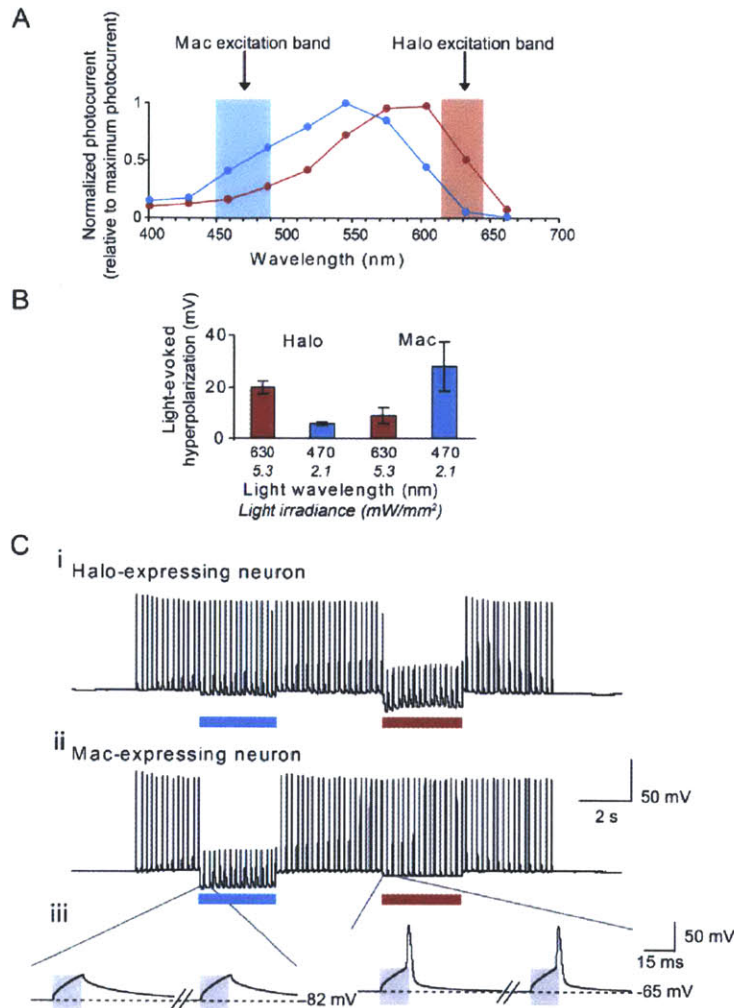


Figure 12 | Multicolor silencing of two neural populations, enabled by blue- and red-light drivable ion pumps of different classes. (A) Action spectra of Mac versus Halo; rectangles indicated filter bandwidths used for multicolor silencing *in vitro*. Blue light is delivered by a 470 ± 20 nm filter at 5.3 mW/mm^2 and red light is delivered by a 630 ± 15 nm filter at 2.1 mW/mm^2 . (B) Membrane hyperpolarizations elicited by blue versus red light, in cells expressing Halo or Mac ($n = 5$ Mac expressing and $n=6$ Halo-expressing neurons). (C) Action potentials evoked by current injection into patch-clamped cultured neurons transfected with Halo (top) were selectively silenced by the red light, but not by the blue-light and vice-versa in neurons expressing Mac (Middle). Grey boxes in the inset (bottom) indicate periods of patch-clamp current injection. (Figure adapted from Chow *et al.* 2010⁵¹)

2.5 Discussion

Arch and Mac represent members of a new, diverse and powerful class of optical neural silencing reagent: the light-driven proton pump. The efficacy of these proton pumps is surprising, given that protons occur at a million-fold lower concentration in mammalian tissue than the ions carried by other optical control molecules.

Extensive work has been done in the optogenetic field with the goal of engineering opsin structure to obtain certain properties. However, this work suggests that a much simpler alternative may be mining ecological and genomic diversity to find naturally-occurring molecular reagents. These opsins may possess desirable properties difficult to engineer, such as the proton pumps' spontaneous recovery after optical activation, and their wide diversity lends itself to spectral diversity which would enable the multiple-color control of independent, discrete neuron populations. Further, structure guided mutagenesis of Arch and Mac may further facilitate the development of neural silencers with altered spectrum or ion selectivity, and lends itself to a better understanding of proton pumps, as well as the larger opsin family.

3. ArchT: a novel, high-light sensitivity neural silencer

The work outlined in this chapter resulted in the publication of “A High-Light Sensitivity Optical Neural Silencer: Development and Application to Optogenetic Control of Non-Human Primate Cortex” in *Frontiers in Systems Neuroscience* (2011) by Xue Han and colleagues⁷². My contribution to this project was in the area of gene cloning, virus making, cell culture transfection, and assessing the effect of different protein trafficking sequences.

3.1 Engineering Arch

In our previous work, we found that the light-driven outward proton pump archaerhodopsin-3 (Arch) was capable of mediating strong, reliable, and safe neural silencing in response to green-yellow light, likely due to its good functional expression in neurons, fast photocycle, rapid post-illumination recovery kinetics, and the excellent proton handling capability of neurons⁴⁰. We next embarked upon a number of strategies to improve Arch including targeted residue mutagenesis, the addition of trafficking sequences, and additional phylogenetic screening. While targeted mutagenesis either significantly reduced or did not alter Arch photocurrents (data not shown), we explored the neural silencing capability of opsins with a high sequence homology to Arch, cloned from various archeal species within the *Halorubrum* genus. All electrogenetic members of this opsin class, known as archaerhodopsins, expressed cleanly and well on the neuron cell plasma membrane and demonstrated large hyperpolarizing currents when expressed in primary rodent neuron culture (Figure 13).

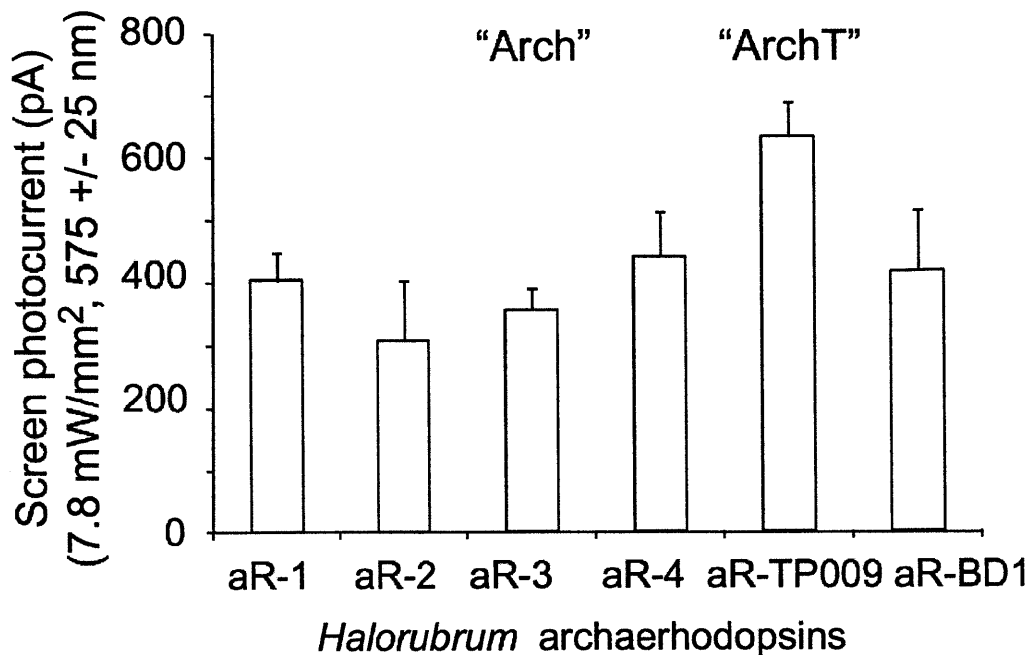


Figure 13 | Archaerhodopsin screen photocurrents. Screen photocurrents generated by various opsins within the archaerhodopsin class, as assessed in neuron culture ($n = 5-16$ neurons for each bar), measured by whole-cell voltage clamp under 7.8 mW/mm^2 , $575 \pm 25 \text{ nm}$ illumination. Full names from left to right: archaerhodopsin from *Halorubrum* strain aus-1 (aR-1), archaerhodopsin from *Halorubrum* strain aus-2 (AR-2), archaerhodopsin from *Halorubrum sodomense* (Arch), archaerhodopsin from *Halorubrum* strain xz515 (aR-4), archaerhodopsin from *Halorubrum* strain TP009 (aR-TP009, aka ArchT), archaerhodopsin from *Halorubrum xingjianense* (aR-BD1). (Figure adapted from Han *et al.* 2011⁷²)

Like Arch, all of the screened archaerhodopsins exhibited rapid photocurrent rise and fall kinetics during illumination, as well as good post-illumination recovery (data not shown). All of the archaerhodopsins exhibited similar action spectra to that of Arch and were proton pumps as evidenced by photocurrent in the absence of sodium, potassium, calcium and chloride ions. The archaerhodopsin from *Halorubrum* strain TP009, which we named ArchT, had the highest of all screened photocurrents. Although Arch and ArchT have highly similar sequences which are homologous by 91.9% (Figure 14), ArchT has an action spectrum slightly red-shifted relative to

Arch and exhibits a 3.3-fold increase in light sensitivity over Arch (Figure 15), with a similar maximum current to Arch (~900 pA *in vitro*) and similar photocurrent rise and fall kinetics.

```

Arch      MDPIALQAGYDLLGDGRPETLWLGIGTLLMLLIGTFYFLVRGWGVTDKDAREYYAVTILVP 60
ArchT    MDPIALQAGYDLLGDGRPETLWLGIGTLLMLLIGTFYFIVKGWGVTDKEAREYYSITILVP 60
          *****:*****:*****:*****

Arch      GIASAAYLSMFFGIGLTEVTVGGEMLDIYYARYADWLFTTPLLLLDLALLAKVDRVTIGT 120
ArchT    GIASAAYLSMFFGIGLTEVTVAGEVLDIYYARYADWLFTTPLLLLDLALLAKVDRVSIGT 120
          *****_******

Arch      LVGVDALMIVTGLIGALSHTAIARYSWWLFSTICMIVVLYFLATSLRSAAKERGPEVAST 180
ArchT    LVGVDALMIVTGLIGALSHTPLARYSWWLFSTICMIVVLYFLATSLRAAAKERGPEVAST 180
          *****_******

Arch      FNTLTALVVLVLTAYPILWIIGTEGAGVVGLGIETLLFMVLDVTAKVGFGFFILLRSRAIL 240
ArchT    FNTLTALVVLVLTAYPILWIIGTEGAGVVGLGIETLLFMVLDVTAKVGFGFFILLRSRAIL 240
          *****

Arch      GDTEAPEPSAGADVSAAD 258
ArchT    GDTEAPEP----- 248
          *****

```

Figure 14 | Arch and ArchT have significant sequence homology. Alignment was done using the ClustalW2 pairwise sequence algorithm created by Thompson and colleagues⁷³.

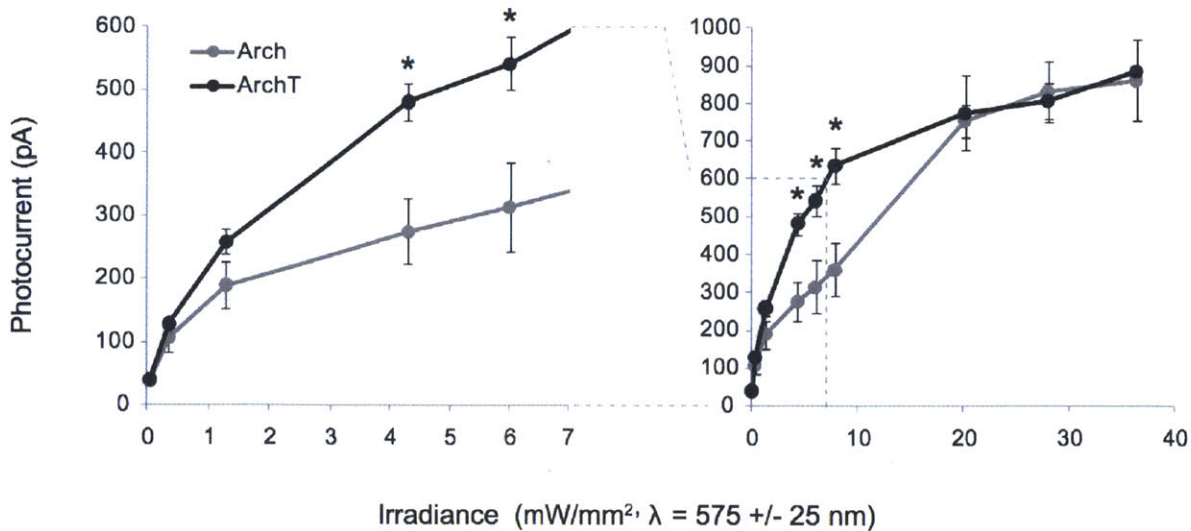


Figure 15 | ArchT is a novel, high-light sensitivity optical neural silencer. Photocurrents of Arch and ArchT measured as a function of 575 ± 25 nm irradiance ($n = 4-16$ neurons for each point); curves are Hill plots. (Figure adapted from Han *et al.* 2011⁷²)

We did not examine irradiances greater than 36.3 mW/mm^2 (the rightmost datapoint in Figure 15), but we would expect a similar maximum degree of inhibition between neurons expressing Arch and ArchT, but a significantly larger silenced brain volume with ArchT given that irradiances as high as $200\text{-}500 \text{ mW/mm}^2$ are used *in vivo*. According to our earlier computational models (Figure 10), a three-fold improvement in light sensitivity would increase the tissue volume addressed by a typical single optical fiber two-fold, making ArchT of instant utility for silencing larger brain volumes. From this, we concluded that ArchT could mediate fast hyperpolarization of neurons with excellent light sensitivity.

3.2 ArchT implementation in the *in vivo* rodent and primate brain

We next made ArchT lentivirus, targeting expression to cortical pyramidal neurons of the murine brain under the CamKII promoter. We found that ArchT trafficked well to the cell membrane and, additionally, expressed rapidly and well along axonal projections traveling far from the cell body, suggesting possible utility in silencing defined projection pathways between different brain regions.

Encouraged by ArchT's high-light sensitivity and good trafficking, coupled with the success of earlier optogenetic non-human primate experiments⁷⁴, we used the aforementioned lentivirus to genetically target ArchT to cortical pyramidal neurons of the cortex of the rhesus macaque. Histological examination of ArchT-expressing neurons in cortical tissue from one monkey showed that neurons appeared healthy and expressed ArchT well at a timepoint 1 month after viral injection (data not shown). When cortical neurons in a second monkey were recorded during illumination with a fiber coupled to an inexpensive 532 nm laser (fiber tip irradiance 100-200 mW/mm²) 1-3 months after viral injection, clear ~100% light-mediated silencing of neural activity was observed in the majority of recorded cells (**Figure 16a, b**) with a median resultant firing rate of 0 spikes/s among the neurons which showed any decrease in firing upon light delivery (**Figure 16c**).

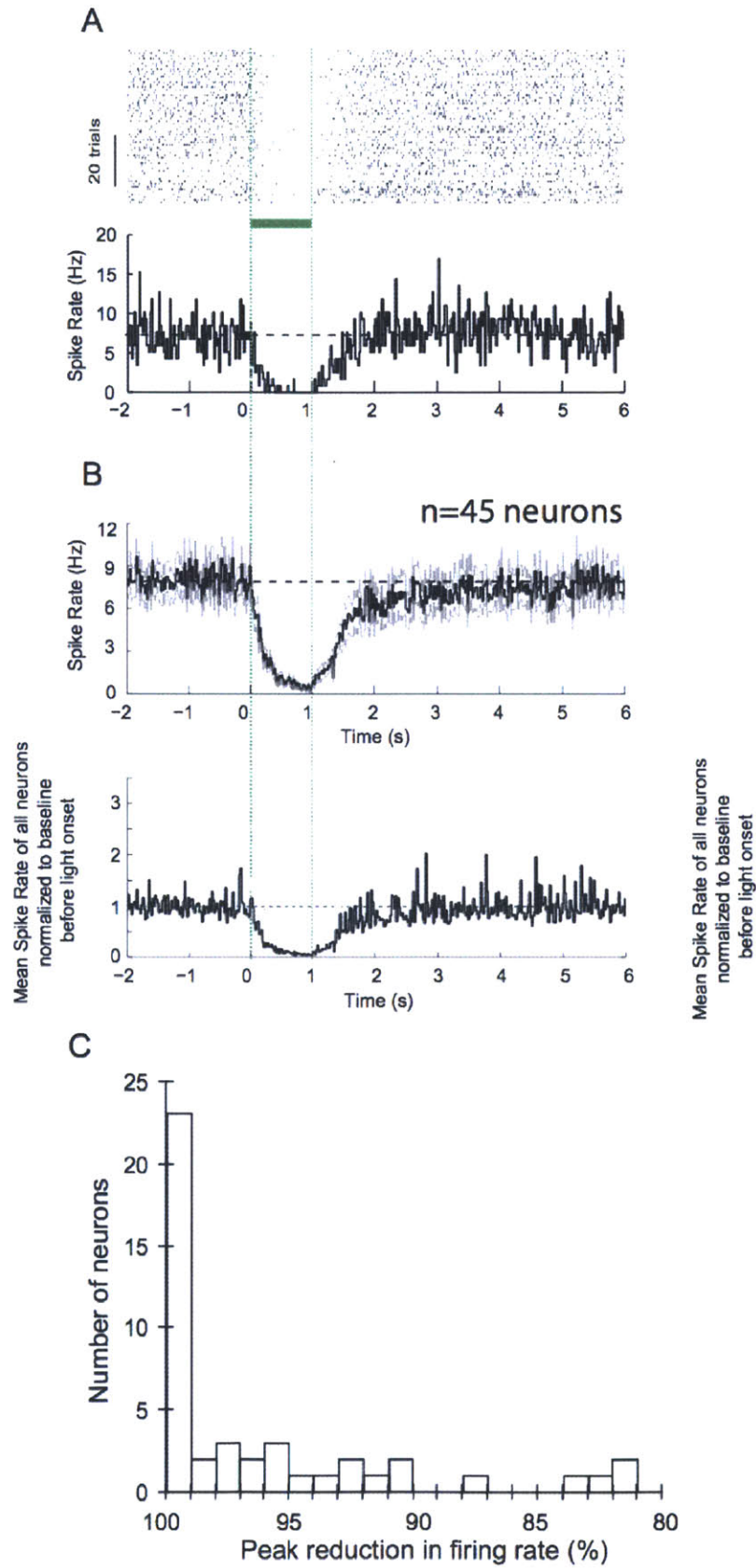


Figure 16 | ArchT-mediated silencing of cortical neurons in the awake

primate brain. (A) Neural activity in a representative silenced neuron in the primate brain before, during and after 1 s of green light illumination. Neural activity shown as a spike raster plot (top), and as a histogram of instantaneous firing rate averaged across trials (bottom; bin size 20 ms). (B) Histogram of instantaneous firing rate, averaged across all silenced single units recorded upon 1 s green light exposure either using raw firing rate data (top) or using firing rate data normalized to baseline firing rate (bottom). (C) Histogram of peak percentage reductions in spike rate, for each individual silenced neuron. (Figure adapted from Han *et al.* 2011⁷².)

Interestingly, 7 of the 74 recorded neurons did not show reductions in firing rate during illumination but instead underwent significant increases in spiking activity during light-delivery to ArchT expressing pyramidal neurons. These cells increased their firing rate by a median of 2.9 fold (range 2.0- to 10.6-fold; Figure 17). These neurons began spiking with a latency of 280 ms after light onset, significantly longer than the latency for initiating optical quieting of the primary population of light-silenced neurons ($p < 0.01$, Mann-Whitney U-test). These increased-activity neurons were recorded at locations that were interspersed amongst the locations where silenced neurons were recorded.

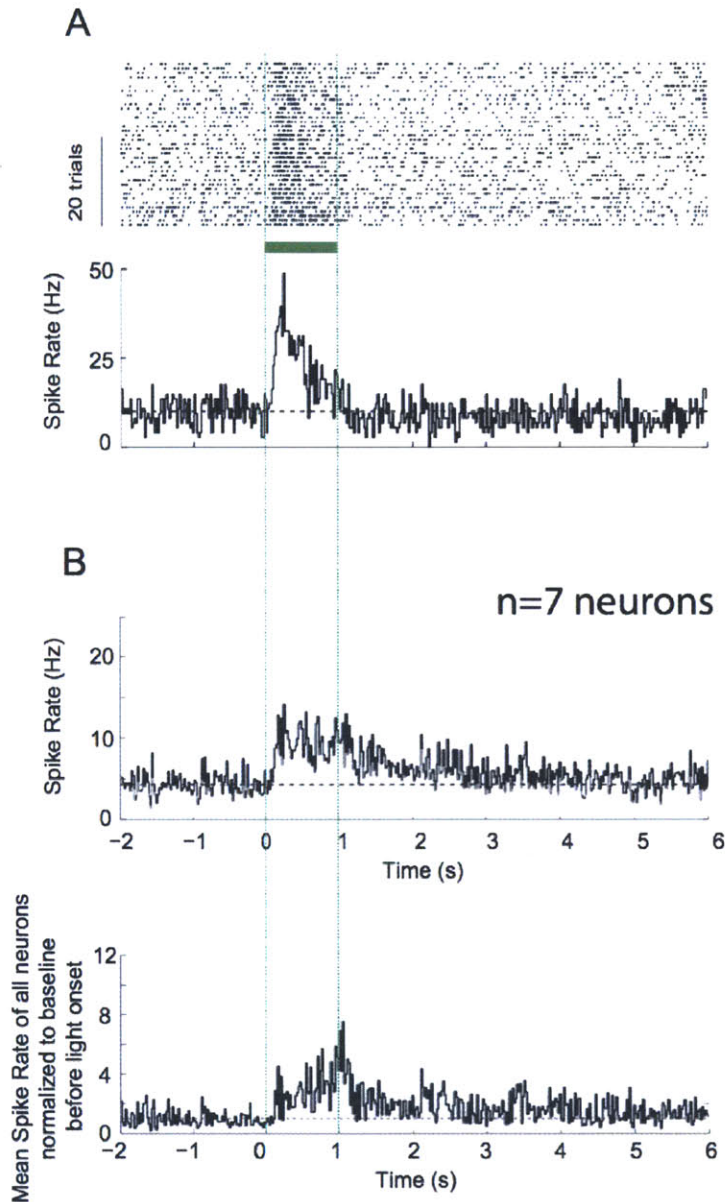


Figure 17 | ArchT silencing causes a firing-increase in a small percentage of neurons. (A) Neural activity, shown as a spike raster plot (top) and as a histogram of instantaneous firing rate averaged across trials (bottom; bin size 20 ms). (B) Histogram of instantaneous firing rate, averaged across all increased-activity single units recorded upon 200 ms green light exposure, either using raw firing data (top) or using firing rate data normalized to baseline firing rate (bottom). Black line, mean; gray lines, mean \pm standard error; $n=7$ increased activity single units. (Figure adapted from Han *et al.* 2011⁷².)

We used spike waveform shapes to analyze the cell-type identity of the silenced and increased-activity neurons. Six of the 45 silenced neurons had narrow spike waveforms with trough-to-peak durations of 100-200 microseconds, suggestive of putative inhibitory neurons, whereas the remainder had broader spike waveforms, suggestive of putative excitatory neurons⁷⁵. Three of the seven increased-activity neurons had narrow spike waveforms, suggestive of inhibitory neurons⁷⁵. Thus, it is likely that both the silenced and increased-activity populations of neurons comprised mixed populations of pyramidal cells and inhibitory cells.

3.3 Discussion

We here present a novel optical neural silencing tool that expresses well on the neuron cell membrane, with good axonal expression, and operates well in the context of the awake mammalian brain. Like Arch, ArchT supports light-driven quieting of neural activity with high efficacy and fast kinetics, utilizing inexpensive 532 nm lasers for illumination. The key difference is that ArchT has >3x improved light sensitivity relative to Arch at lower light powers from 1-10 mW/mm², something of critical importance for silencing large brain volumes with a single fiber: a system in which light falls off rapidly and geometrically.

4. Synthetic Physiology: Strategies for Adapting Tools From Nature

This chapter was published elsewhere as “Synthetic physiology strategies for adapting tools from nature for genetically targeted control of fast biological processes” in *Methods in Enzymology* (2011) by Brian Chow, myself, Nathan Klapoetke and Edward Boyden⁷⁶.

4.1 Molecular design and construction

We here identified a number of opsins from genomic databases by searching for proteins with similar amino acid sequence homology to previously characterized opsins. This method can be extrapolated to the larger goal of developing synthetic physiology tools. A number of microbial opsins have been identified at a genomic level in the forty years since the class was first identified, yet only a subset of these molecules have been characterized at a physiological level. *De novo* gene synthesis has proven important for rapid construction of opsin DNA from sequences derived from genomic and transcriptomic databases^{2,40}. One can obtain a gene codon-optimized to the target organism^{77,78,79} within a few days to weeks of sequence identification. Codon optimization is useful for heterologous expression of these genes, which are originally isolated from algae, bacteria, and other non-animal species. *De novo* gene synthesis additionally allows the elimination of restriction sites within the gene to ease later molecular cloning steps, for example, by enabling fusion of a fluorescent protein tag to the molecule, adding trafficking sequences, or adding a cell type-specific promoter to the gene to delimit the expression to specific cells within the target organism.

After gene synthesis, the next step is to alter the gene as needed, or to append extra sequences to optimize its function toward a directed physiological control goal. A few opsin crystal structures have been obtained^{80,37,36,81,82,83} and decades of studies have been performed in which specific residues within opsins were mutated, followed by spectroscopic or physiological characterization of the resultant mutated opsins^{84,49,50,85,48,47,86,87,88,89,90,51}. These datasets have proven influential in guiding the strategic engineering of these molecules through site-directed mutagenesis^{91,92,93,40,94}, enabling the creation of molecules with improved trafficking, or faster or slower kinetics. Antibodies for localizing many of these opsins in an immunocytochemical

fashion are not yet commonly available, so tagging the proteins with a fluorophore or a known antibody epitope is helpful to efficiently determine which cells within the target organism are expressing the opsin. Such tagging additionally yields critical information about the membrane trafficking and localization of opsins within cells – indeed, fluorophore localization to the plasma membrane of opsin-fluorophore fusions has been used to predict photocurrent magnitude, as measured through electrophysiology characterization^{40,93}.

We have previously reported a method for quantifying membrane localized proteins in neurons⁴⁰, based on a Gaussian-blur-based technique developed for the same purpose in HEK293 cells⁹³. This method is useful for quantifying protein localization in the cells, but it does not provide information on whether the protein is properly folded and functional within the membrane. Ultimately it is the number of functional proteins in the membrane which determines their overall physiological control efficacy. Since these molecules, when expressed in neurons or other animal cells, are often in a very different lipid environment than the one they evolved to function in, even a properly folded molecule in a lipid membrane may not be fully functional. As a concrete example, photocurrent enhancement of an opsin by appending the flanking sequences of the Kir2.1 protein⁹⁵ boosts the membrane expression of opsins as observed through microscopy, but may boost the photocurrent even more than might be expected from the cellular appearance alone: this appearance-current discrepancy may vary from opsin to opsin. Indeed, Kir2.1 sequences may even decrease overall cellular expression for some opsins, even as it increases the amount of properly folded functional membrane-embedded protein. Thus, quantitative confocal microscopy must be supplemented by a functional, physiological assay. This theme -- that there are few proxies for function in the assessment of synthetic physiology tools -- is partly why they are hard to find, engineer, and assess.

It is important to realize that the complexity of these molecules means that even an innocuous change like creating a fusion protein between an opsin and a fluorophore may modulate the function of the opsin. Several laboratories have observed that fluorophore fusions with a target molecule can alter performance of the target molecule by altering viral titer⁹⁶. Appending different fluorophores (e.g., EGFP vs. mCherry vs. ECFP) to an opsin can result in different appearances (e.g., due to mCherry's greater tendency to aggregate than EGFP or ECFP) and

potentially different photocurrent for a given cell type. In the event that fusion of a fluorophore to a given opsin is undesirable, alternatives exist to directly fusing fluorophores to opsins, while still enabling identification of cells expressing the opsin, including interposing IRES (internal ribosome entry sites) or 2A sequences ('self-cleaving' linkers first identified in foot-and-mouth-disease virus) between opsins and fluorophores. Protein expression levels for the gene that appears after the IRES is often a small fraction of that of the gene before the IRES^{97,98,99,100}. 2A sequences in principle yield highly stoichiometric amounts of translated protein, but in reality, different functional levels may be observed for the pre- and post-2A proteins, due to alterations in protein trafficking or function that result from the residual amino acids of the 2A sequence left behind after protein translation^{41,101}.

The use of trafficking sequences, export motifs, and other signal sequences is useful for improving the heterologous expression of opsins in the cells of target organisms, since the function of opsins in neurons is primarily achieved when opsins express on the plasma membrane. Practically all opsins come from organisms whose membrane structure and overall cellular architecture is different from neurons. For example, *N. pharaonis* halorhodopsin photocurrents can be enhanced several fold in mammalian cells by appending the N- and C-terminal sequences of the human Kir2.1 potassium channel protein, which are responsible for endoplasmic reticulum-export and Golgi-export (although, see alternative explanations of the role that these Kir2.1 sequences play in boosting cellular expression, above)^{102,103,104,95}. The enhancement offered by a given exogenous trafficking sequence is opsin-dependent. A trafficking sequence that boosts *N. pharaonis* halorhodopsin expression levels (the ER2 sequence⁵⁴) has no effect on improving the currents of the *H. sodomense* archaerhodopsin-3, although adding a different sequence (the Prl sequence, derived from the prolactin secretion targeting sequence) does improve archaerhodopsin-3 expression and photocurrent⁴⁰. Through experimenting with combinatorial addition of N- and C-terminal signal sequences, we have found adding multiple signal sequences does not necessarily improve expression in a linear way, perhaps owing to interactions between the multiple trafficking mechanisms at play. It should be noted that opsins may also possess intrinsic, even covert, sequences that enable them to be expressed very well on the plasma membrane. For example, the light-driven outward proton pump archaerhodopsin-3 from *H. sodomense* (and, in general, members of the archaerhodopsin

class of opsins) naturally expresses rapidly and well on plasma membranes⁴⁰. Opsin mutagenesis and chimeragenesis has pointed towards candidate amino acids that may play a critical role in opsin trafficking and expression on the plasma membrane^{92,93}.

4.2 Transduction of microbial opsins into cells for heterologous expression.

The analysis of the potential power of a given microbial opsin to control the voltage or ionic composition of a target cell type should ideally be performed in the target cell type itself, or in a testbed cell type as similar as possible to the target cell type. For example, the trafficking-enhancement and protein folding enhancement sequences described above are derived from specific species, and were optimized in cells from specific species; accordingly, they may not work equally well in species different from the source species, or in cell types greatly different from the cell types used to assess and optimize the sequences. Similarly, the covert trafficking sequences found within opsins may not function equally well in all cell types. As a concrete example, the *H. salinarum* bacteriorhodopsin has long been considered a difficult protein to express in *E. coli*¹⁰⁵, but it expresses readily in mammalian neurons, and can mediate biologically meaningful photocurrents⁴⁰. Similarly, channelrhodopsin-2 does not express well in *E. coli*, but expresses well in mammalian neurons. Conversely, proteorhodopsins from uncultured marine gamma-proteobacteria express and function well in *E. coli*, but do not generate photocurrents in HEK293 cells or mouse neurons⁴⁰, despite a rudimentary degree of expression of the proteorhodopsin protein in these mammalian cells. Thus, reliance on a single heterologous expression cell type (e.g., *E. coli*, yeast, *Xenopus* oocytes, HEK cells) as the sole testbed for characterizing opsin physiological function, may lead to a partial picture of how well the opsins assessed will perform across the broad set of cell targets confronted in biology. Similarly, screening for enhancing mutations, trafficking sequences, or other beneficial modifications, using a single heterologous expression cell type, may lead to unintentional optimization of the opsin for function in that particular cell type, and potential deoptimization of expression, trafficking, or function in other cell types of interest within the ultimate tool usage spectrum.

If mammalian neurons in the living mouse or rat are the target, then mammalian neurons in primary culture should be at some point used to assess the function of a given opsin^{40,1}, although ideally *in vivo* assessment should be performed as well, given the very different state of neurons *in vivo* vs. *in vitro*. It is important to note that different types of neurons, at different ages, may well differ in their level and timecourse of opsin expression and function. We typically utilize

mouse hippocampal and cortical primary cultures because they contain representatives of some of the major cell classes in the brain¹. However, primary neuron cultures are laborious to prepare and maintain, and so we and others use HEK293 cell lines to perform electrophysiological characterization of opsins^{40,92,106,93}. HEK cells are more robust, and easier to work with, than neurons, and can be grown for multiple cell division cycles in culture, unlike neuron cultures which do not replicate after plating and differentiation. In addition, HEK cells possess cellular shapes and molecular phenotypes that are somewhat less variable than those of neurons, and possess fewer active conductances than do neurons; both of these features help reduce variability of opsin characterization measurements. Conversely, HEK cells may yield smaller photocurrents than do neurons due to their smaller surface area, and may have limited utility in fully predicting how well a protein will traffic in neurons. As a simple example of this latter point, HEK cells do not possess axons or dendrites; some findings have been published claiming that certain opsins preferentially traffic to the synaptic processes of neurons¹⁰⁷, and any such effects would not be observable in a HEK cell. However, HEK cells are still extremely useful for performing fast screening assays of whether there is any physiological effect of illuminating a given opsin, and may be particularly useful for characterization of amplitude-normalized features of opsins such as the action spectrum, the plot of the relative photocurrent observed upon delivery of light of different colors.

Transfection is the simplest and fastest way to get DNA that encodes for opsins into cells, for rapid characterization of opsins in a cellular context. For HEK cells, transfection can increase the likelihood of delamination from the substrate; the use of Matrigel to promote cell adhesion to a glass coverslip when plating, as opposed to poly-lysine, is suggested. Well-dissociated HEK cells that are spatially separated from one another are critical for high-quality electrophysiological assays, as HEK cells that grow together can form gap junction-connected syncytia that can preclude accurate electrophysiological analysis of expressed opsins, by compromising voltage-clamp fidelity. In order to improve the quality of HEK cells for physiological assessment, passage the cells for their final plating when they reach medium levels of confluence (~50%); then, during the final plating step, trypsinize the HEK cells, resuspend the cells in serum-free media and pipette the cells against the sidewalls of the dish or flask to break up clumps of cells, perhaps triturating the cells with a fine-gauged sterile needle (e.g., <5 times

to avoid excessive mechanical force on cells, through a ~31 gauge needle), and then add serum-containing media (to halt the trypsinization) before plating the final mixture on glass coverslips. For neuron culture, mouse or rat hippocampal or cortical neurons should be cultured from P0 pups or E18 embryos at moderate densities, using standard protocols⁴⁰. Multiple experimenters in our laboratory have independently found that the best recordings from opsin-expressing neurons are often from ones in areas of sparse neuron density, often at the edge of the area occupied by cells. The preferred method for HEK and neuron culture transfection is calcium phosphate precipitation of DNA, e.g. using commercially available kits. The calcium phosphate precipitation-based process can be harsh on neurons; accordingly, precautions should be taken. The best transfection rates in neurons, in our hands, are achieved when neurons are transfected 3-4 days *in vitro*, with rapidly diminishing efficiency beyond then (although the genes encoding for quickly and highly expressed proteins, like Arch, can be delivered at 5 days *in vitro*).

Viral vectors can also be useful for assessing opsin function, because they can result in a high yield of opsin-expressing cells in a cultured cell environment, and they can also be used to insure a precise gene dosage into a cell of interest. They present lower neuron toxicity at a higher cellular yield than can commonly be achieved with calcium phosphate transfection. One key consideration is that recombination can be a major issue when preparing viral vectors, due to the presence of repetitive sequences within the genomic vector of the virus, i.e. the payload-encoding plasmid. In theory any *E. coli* with loss of function mutation in *rec* gene(s) should be suitable for growing up such plasmids. However in our experience working with lentiviral plasmids, Stb13 (*recA13-*) *E. coli* have a much lower rate of recombination compared to other *rec-* cells such as XL1-Blue (*recA1-*). XL10-Gold *E. coli* may work as well, with AAV plasmids. It is recommended to try out different types of *rec-* cells to find the optimal one for a particular viral vector, as recombination events can cause loss of vectors, and require time-consuming plasmid reconstruction. It is also important to check if any special considerations are needed for utilizing these specialized viral plasmid-optimized competent cell lines. For example Stb13 is *endA+*, and thus the *endA* endonuclease will need to be removed with appropriate washing when purifying the DNA, to prevent DNA degradation. To check for recombination, viral plasmids should regularly be verified in both sequence and topology, using DNA sequencing and restriction digestion respectively. Both methods are recommended because

sequencing short regions, such as the cloned insert, will only inform whether the sequence is locally correct, while recombination can occur between unpredictable locations, so that the cloned sequence is largely locally correct but different in global topology. Therefore it is highly recommended to perform multiple restriction digests to verify that the global sequence topology has not deviated from the designed plasmid. When cloning payloads into viral vectors, it is important to use only parent vectors that have also been tested for recombination, and it is important to perform both sequencing and restriction digests periodically as a viral plasmid stock is generated and propagated, ideally minimizing the number of generations that a stock is propagated to the minimum possible.

4.3 Physiological assays

Once a molecule is chosen, and expressed in a target cell type for characterization, it must be physiologically characterized by an observation method (e.g., patch clamp, dye imaging) – in the case of opsins, using illumination. Below we discuss illumination hardware, solutions in which to perform experiments, strategies for selecting cells to be analyzed, and methods for cellular readout.

The millisecond-scale resolution of optogenetic tools enables the remote control of cellular physiology with unprecedented resolution, but also requires illumination sources with increased temporal resolution than what is achievable with conventional fluorescence illuminators. A commonly used programmable excitation source is the Sutter DG-4, which uses a galvanometer mirror to direct light from the lamp into one of four filter slots within the lamp in order to determine the excitation wavelength. A second mirror is used to shutter and/or adjust the intensity of light by modulating how much is directed to the light collection optics for delivery from the DG4 into the microscope. The output of the DG4 can be fed into an illuminator port of practically any microscope used for fluorescence imaging or electrophysiology. Laser based systems are also useful; since the action spectra of microbial rhodopsins are quite broad, typically with 100-150 nm bandwidths (full-width at half-maximum), sub-optimal excitation at a given wavelength of illumination can easily be compensated for by increased illumination power. For example, a 532 nm solid-state green laser is an order of magnitude cheaper than a 593 nm solid-state yellow laser, but will still excite the yellow light-sensitive *N. pharaonis* halorhodopsin quite effectively, just by increasing the delivered power slightly over the amount that would be required if a 593 nm laser were used. Action spectra (but not true absorbance spectra, which requires flash photolysis) can be measured during electrophysiological recording, by scanning through the visual spectrum with a Till Photonics Polychrome V or analogous color-programmable light source, coupled to a microscope through a standard fiber optic cable. In this particular illuminator, broadband light from a xenon lamp is passed through a programmable monochromator, so as to emit light with narrowband (10 nm bandwidths) properties, centered at various wavelengths. Light-emitting diodes (LEDs) have become increasingly popular due to their cheapness and fast switching times; a recent report¹⁰⁸ offers excellent instructions for

constructing a high-power and fast illuminator with two LEDs co-aligned for dual-spectral excitation, and commercial systems from Thorlabs and other vendors are also available. Most LEDs can be switched on and off with very fast (e.g., nanosecond) resolution, so the temporal resolution of various LED systems is largely limited by the drivers or power sources. LEDs are particularly useful for ultraviolet, orange, red, and infrared wavelengths, since many lamps are only weakly irradiant in these spectral bands.

Solutions used in electrophysiological characterization of mammalian cells (e.g., during patch clamp or imaging) are in some ways more complicated than typical solutions used in molecular biology. We highly suggest preparing electrophysiology solutions from scratch, instead of purchasing pre-made solutions. These solutions must be osmotically balanced to prevent cell death, ideally within 1-5 mOsm, and pH balanced, ideally within 0.1 pH units; extreme precaution must be taken to avoid contamination of reagents (as even a small change in a low-concentration ion, like calcium, can greatly change the health or electrical properties of a cell under electrophysiological study). For example, our laboratory (and many other electrophysiology laboratories) avoid insertion of spatulas into stock containers to dispense solids for preparing electrophysiological solutions; chemicals are instead poured from stock containers whenever possible. Solutions should be sterile filtered immediately following preparation, to maximize cell health and available recording time, as use of sterile aliquots of solutions can improve cell health. Our bath solution of choice for *in vitro* experiments using both HEK cells and neurons is Tyrode's solution, a HEPES buffer-based saline solution¹. Artificial cerebrospinal fluid (ACSF), which is bicarbonate-buffered, may improve cell health in certain circumstances over that obtained from use of Tyrode's Solution, but requires fluid manifolds to perfuse CO₂-saturated solutions in order to maintain physiological pH levels, and the added inconvenience is often not justified. For the use of dyes that indicate the levels of ions such as H⁺ or Ca²⁺ (e.g., SNARF, fura-2, Oregon Green BAPTA), the manufacturers' instructions provide a good starting point for deriving protocols for the loading and imaging of the dyes, although some optimization of loading conditions and imaging conditions may be required for given cell types and given conditions of joint photostimulation and imaging^{40,92,109}.

Even within a cell type, different cells will vary in their levels of opsin expression, appearance, and sustained photocurrents, potentially to great degrees. Excessive overexpression of an opsin can lead to poor cell health, so simply picking the very brightest cells to record electrophysiologically may yield unrepresentative data, and accurate characterization of the performance of an opsin ideally is performed with unbiased selection of cells. Beginning experimenters may have slightly different, even unconscious, biases in cell choice strategy, e.g. choosing the biggest cells in the field of view. To address some of these problems, we often normalize observed photocurrents by cell capacitance, thus obtaining the photocurrent density, which helps compensate for the varying size of the cells being recorded.

Expression of opsins in a cell can increase over time, as the process of protein expression and trafficking can be slow. For full characterization of an opsin, it is recommended to assess opsin function at various times after transfection, e.g. between a few days and a few weeks, to understand the timecourse of expression and trafficking. Importantly, different opsins, and opsins expressed using different gene delivery mechanisms, will present with different timecourses of functional expression. In neurons, we have noted a trend for many microbial rhodopsins from archaea to express and traffic to the membrane more quickly than do those from fungus and plants, although specific opsins within these families can violate this trend. Typically, the photocurrents measured in neurons from archaeal rhodopsins (both bacteriorhodopsins and halorhodopsins) using the protocols in Section IV do not change after 5-6 days post-transfection or 10 days post-viral infection; photocurrents of channelrhodopsin-2 take a few extra days to plateau, compared to the archaeal opsins. These are the times that it takes for currents to saturate; fluorescence levels may saturate much earlier, perhaps because although opsins are rapidly expressed at the level of protein, it may take some time for them to traffic, and assemble within the membrane in functional form (e.g., some may potentially require multimerization within the membrane to attain full function). It is possible that adding trafficking sequences, or inducing mutations, can result in slowed down or sped up functional protein expression, versus the wild type form of the opsin.

Similar trends in expression and membrane localization rates as a function of kingdom of origin area also observed in transfected HEK cells, with faithful expression of rhodopsins from archaea

requiring two days and ones from fungi and plants requiring up to three days (although again, individual opsins may violate these rules of thumb). These multi-day expression times may present difficulties because HEK cells will divide a few times during this period, and this counteracts the goal of performing reliable recordings on isolated cells (or on cells with minimal shared membrane with other cells, as described in Section III). The addition of sodium butyrate¹¹⁰ or lowering the cell culture incubator temperature (32°C instead of 37°C) can extend the time between cell divisions and allow for more time for membrane expression⁹³.

4.4 Conclusion

The process of assessing the physiological function of a heterologously expressed protein in a target cell is complex. Such explorations are critical for understanding the potential uses of a given synthetic physiology tool, for evaluating potential side effects or toxicity of a candidate tool, or for screening for novel or optimized tools. As a closing example, it was originally believed that channelrhodopsin-1 (ChR1) was a light-gated proton channel, but multiple reports since then have demonstrated that it is indeed a nonspecific cation channel like ChR2 when evaluated at neutral pH and expressed at sufficiently high levels^{93,111}. Thus, considerations of the cellular environment in which a protein is evaluated, e.g. pH and expression level, are key for understanding the physiological power of a given molecular tool. In summary, assessing the function of a given physiological driver is complex because of the many variables that can modulate the expression and performance of physiological drivers, and the quantitative, high-speed nature of the signal being driven. The creation of new model systems that can replicate key features of targeted physiological systems, in a fashion that could support high-throughput tool assessment or tool optimization, may greatly enhance the ability to generate novel and impactful synthetic physiology tools.

5. Summary and Further Work

The life and operation of cells involve physiological processes that take place over fast timescales of milliseconds to minutes. Technologies for driving or suppressing specific fast physiological processes in intact cells are critical for the ability to understand how those physiological processes contribute to emergent cellular and organismal functions and behaviors. Understanding and engineering optogenetic tools requires thinking and working at the level of protein structure and dynamics.

A diversity of molecular tools have been developed which enable the precision control of neural processes. We here present three novel optical silencers identified through an exploration of phylogenetic diversity. Arch, Mac, and ArchT enable the powerful optically-mediated silencing of the *in vivo* mammalian brain, as well as the multiple-color control of independent neuron populations.

For the future, the identification of opsins which possess blue or red shifted action spectra would be of great use to the neuroscience community. Opsins with spectrally distant action spectrum enable the bidirectional control of single cell types, or the multiple color control of independent cell populations with a minimum of cross-excitation. Additionally, a major barrier to *in vivo* silencing is the light power attenuation created by tissue and hemoglobin optical absorption. This optical attenuation is dramatically reduced at red wavelengths, suggesting that red light is able to propagate further in the brain than other wavelengths, and thus enable the silencing of much larger brain volumes. Thus, the engineering of optical hyperpolarizers may enable the long-distance and less invasive inactivation of neural activity in the mammalian brain and is at present an area of great interest.

6. Experimental Methods

6.1 Plasmid construction and site directed mutagenesis.

Opsins were mammalian codon-optimized, and synthesized by Genscript (Genscript Corp., NJ). Opsins were fused in frame, without stop codons, ahead of GFP (using BamHI and AgeI) in a lentiviral vector containing the CaMKII promoter, enabling direct neuron transfection, HEK cell transfection (expression in HEK cells is enabled by a ubiquitous promoter upstream of the lentiviral cassette), and lentivirus production (except for *Halobacterium salinarum* halorhodopsin, which was fused to GFP in the vector pEGFP-N3 (using EcoRI and BamHI) and only tested by transfection). eNpHR was synthesized as described before, by inserting the signaling sequence from the acetylcholine receptor beta subunit (amino acid sequence: MRGTPLLLVVSLSLLQD; DNA sequence: atgaggggtacgccctgctcctcgtcgtctctctgttctctctgcttcaggac) at the N-terminus, and the ER2 sequence (amino acid sequence: FCYENEV; DNA sequence: ttctgctacgagaatgaagtg) at the C-terminus of Halo.

The 'ss' signal sequence from truncated MHC class I antigen corresponded to amino acid sequence (M)VPCTLLLLLAAALAPTQTRA, DNA sequence GTCCCGTGACGCTGCTCCTGCTGTTGGCAGCCGCCCTGGCTCCGACTCAGACGCGG GCC. The 'Prl' Prolactin signal sequence corresponded to amino acid sequence MDSKGSSQKGSRLLLLLVVSNLLLCQVVS, DNA sequence gacagcaaaggttcgtcgcagaaaggtcccgcctgctcctgctgctggtgtgcaaatctactcttgtgccaggggtgtgctccacccc cgtc. Halo point mutants for HEK cell testing were generated using the QuikChange kit (Stratagene) on the Halo-GFP fusion gene inserted between BamHI and EcoRI sites in the pcDNA3.1 backbone (Invitrogen). All constructs were verified by sequencing, and codon-optimized sequences of key opsins were submitted to Genbank (mammalian codon-optimized Arch, GU045593; mammalian codon-optimized Arch fused to GFP, GU045594; mammalian codon-optimized Mac, GU045595; mammalian codon-optimized Mac fused to GFP, GU045596; ss-Prl-Arch, GU045597; ss-Arch-GFP-ER2, GU045598; ss-Prl-Arch-GFP, GU045599) and made available for request at:

<http://syntheticneurobiology.org/protocols>

The amino acid sequence of Halo is:

MTETLPPVTESAVALQAEVTQRELFEFVLNDPLLASSLYINIALAGLSILLFVFMTRGLDD
PRAKLIAVSTILVPVVSIA SYTGLASGLTISVLEMPAGHFAEGSSVMLGGEEVDGVVTM
WGRYLTWALSTPMILLALGLLAGSNATKLF TAITFDIAMCVTGLAAALTTSSHLMRWF
WYAISCACFLV VLYILLVEWAQDAKAAGTADMFN TLKLLTVVMWLGYP I VWALGVEG
IAVLPVGVTSWGYSFLDIVAKYIFAFLLLNYLTSNESVVSGSILDVPSASGTPADD.

The amino acid sequence of Arch is:

MDPIALQAGYDLLGDGRPETLWLGIGTLLMLIGTFYFLVRGWGVTDKDAREYYAVTIL
VPGIASAAYLSMFFGIGL TEVTVGGEMLDIYYARYADWLFTT PLLLLDLALLAKVDRVT
IGTLVGVDALMIVTGLIGALSHTAIARYS WWLFSTICMIVVLYFLATSLRSAAKERGPEV
ASTFNLTALV LVLWTAYPILWIIGTEGAGVVGLGIETLLFMVLDVTAKVGF GFILLRSR
AILGDTEAPEPSAGADVSAAD.

The amino acid sequence of ArchT is:

MDPIALQAGYDLLGDGRPETLWLGIGTLLMLIGTFYFIVKGWGVTDKEAREYY SITILVP
GIASAAYLSMFFGIGL TEVTVAGEVLDIYYARYADWLFTT PLLLLDLALLAKVDRVSIGT
LVGVDALMIVTGLIGALSHTPLARYS WWLFSTICMIVVLYFLATSLRAAAKERGPEVAS
TFNLTALV LVLWTAYPILWIIGTEGAGVVGLGIETLLFMVLDVTAKVGF GFILLRSRAIL
GDTEAPEP.

The amino acid sequence of Mac is:

MIVDQFEEVLMKTSQLFPLPTATQSAQPTHVAPVPTVLPDTP IYETVGDSGSKTLWVVF
VLMLIASAAFTALS WKIPVNRRLYHVITTIITLTAALSYFAMATGHGVALNKIVIRTQHD
HVPD TYETVYRQVYYARYIDWAITP LLLLLDLG LLAGMSGAHIFMAIVADLIMVLTGLF
AAF GSEGTPQKWGWYTIACIAYIFV VVH LVLN GGANARVKGEK LRSFFVAIGAYTLIL
WTAYPIVWGLADGARKIGVDGEIAYAVLDV LAKGVFGAWLLVTHANLRES DVELNGF
WANGLNREGAIRIGEDDGA.

6.2 Neuron culture, transfection, infection, and imaging

All procedures involving animals were in accordance with the National Institutes of Health Guide for the care and use of laboratory animals and approved by the Massachusetts Institute of Technology Animal Care and Use Committee. Swiss Webster or C57 mice (Taconic or Jackson Labs) were used. For hippocampal cultures, hippocampal regions of postnatal day 0 or day 1 mice were isolated and digested with trypsin (1 mg/ml) for ~12 min, and then treated with Hanks solution supplemented with 10-20% fetal bovine serum and trypsin inhibitor (Sigma). Tissue was then mechanically dissociated with Pasteur pipettes, and centrifuged at 1000 rpm at 4°C for 10 min. Dissociated neurons were plated at a density of approximately four hippocampi per 20 glass coverslips, coated with Matrigel (BD Biosciences). For cortical cultures, dissociated mouse cortical neurons (postnatal day 0 or 1) were prepared as previously described, and plated at a density of 100-200k per glass coverslip coated with Matrigel (BD Biosciences). Cultures were maintained in Neurobasal Medium supplemented with B27 (Invitrogen) and glutamine. Hippocampal and cortical cultures were used interchangeably; no differences in reagent performance were noted.

Neurons were transfected at 3-5 days *in vitro* using calcium phosphate (Invitrogen). GFP fluorescence was used to identify successfully transfected neurons. Alternatively, neurons were infected with 0.1-1 μ l of lentivirus per well at 3-5 days *in vitro*. Throughout the paper, neurons were transfected unless indicated as having been infected. All images and electrophysiological recordings were made on neurons 9-14 days *in vitro* (approximately 6-10 days after transfection or viral infection).

Confocal images of infected neurons in culture (briefly fixed in 4% paraformaldehyde) were obtained with a Zeiss LSM 510 confocal microscope (63X magnification objective lens). Culture images were maximum intensity projections made from sets of 5 images (1.0 μ m image plane thickness) spaced along the z-axis by 0.5 micron steps. Quantitative confocal analysis of membrane expression of opsins was performed using infected neurons in culture (10 days post-infection, briefly fixed in 4% paraformaldehyde). Images were obtained with a Zeiss LSM 510 confocal microscope (63X magnification objective lens), always with the same illumination and

observation parameters to avoid procedural variability. Given the near-100% viral infection rate, isolated neurons were chosen for analysis in order to reduce background fluorescence from nearby neurons and their processes. Images were analyzed in ImageJ (National Institutes of Health), based on a neuron-adapted version of a previously reported algorithm used to assay membrane expression of channelrhodopsins and channelrhodopsin variants in HEK cells. An image was first filtered with a 2-pixel Gaussian blur, and the filtered image was subtracted from the original one to enhance the contour of the cell.

6.3 HEK 293FT cell culture and transfection

HEK 293FT cells (Invitrogen) were maintained between 10-70% confluence in D10 medium (Cellgro) supplemented with 10% fetal bovine serum (Invitrogen), 1% penicillin/streptomycin (Cellgro), and 1% sodium pyruvate (Biowhittaker)). For recording, cells were plated at 5-20% confluence on glass coverslips coated with Matrigel (BD Biosciences). Adherent cells were transfected approximately 24 hours post-plating either with TransLT 293 lipofectamine transfection kits (Mirus) or with calcium phosphate transfection kits (Invitrogen), and recorded via whole-cell patch clamp between 36-72 hours post-transfection.

6.4 Lentivirus preparation

HEK293FT cells (Invitrogen) were transfected with the lentiviral plasmid, the viral helper plasmid p Δ 8.74, and the pseudotyping plasmid pMD2.G. The supernatant of transfected HEK cells containing virus was then collected 48 hours after transfection, purified, and then pelleted through ultracentrifugation. Lentivirus pellet was resuspended in phosphate buffered saline (PBS) and stored at -80°C until further usage *in vitro* or *in vivo*. The estimated final titer is approximately 10^9 infectious units/mL.

6.5 Virus injection in the adult mouse.

All procedures were in accordance with the National Institutes of Health Guide for the Care and Use of Laboratory Animals and approved by the Massachusetts Institute of Technology Committee on Animal Care. Under isoflurane anesthesia, 1 μL lentivirus was injected through a craniotomy made in the mouse skull, into the motor cortex (0.62 mm anterior, 0.5 mm lateral, and 0.5 mm deep, relative to bregma), or the sensory cortex (0.02 mm posterior, 3.2 mm lateral, and 2.2 mm deep, relative to bregma). Virus was injected at a rate of 0.1-0.2 $\mu\text{L}/\text{min}$ through a cannula connected via polyethylene tubing to a Hamilton syringe, placed in a syringe pump (Harvard Apparatus). The syringe, tubing, and cannula were filled with silicone oil (Sigma). For mice used for *in vivo* recordings, custom-fabricated plastic headplates were affixed to the skull, and the craniotomy was protected with agar and dental acrylic.

6.6 *In vitro* whole cell patch clamp recording & optical stimulation

Whole cell patch clamp recordings were made using a Multiclamp 700B amplifier, a Digidata 1440 digitizer, and a PC running pClamp (Molecular Devices). Neurons were bathed in room temperature Tyrode containing 125 mM NaCl, 2 mM KCl, 3 mM CaCl_2 , 1 mM MgCl_2 , 10 mM HEPES, 30 mM glucose, 0.01 mM NBQX and 0.01 mM GABAazine. The Tyrode pH was adjusted to 7.3 with NaOH and the osmolarity was adjusted to 300 mOsm with sucrose. HEK cells were bathed in a Tyrode bath solution identical to that for neurons, but lacking GABAazine and NBQX. Borosilicate glass pipettes (Warner Instruments) with an outer diameter of 1.2 mm and a wall thickness of 0.255 mm were pulled to a resistance of 3-9 $\text{M}\Omega$ with a P-97 Flaming/Brown micropipette puller (Sutter Instruments) and filled with a solution containing 125 mM K-gluconate, 8 mM NaCl, 0.1 mM CaCl_2 , 0.6 mM MgCl_2 , 1 mM EGTA, 10 mM HEPES, 4 mM Mg-ATP, and 0.4 mM Na-GTP. The pipette solution pH was adjusted to 7.3 with KOH and the osmolarity was adjusted to 298 mOsm with sucrose. Access resistance was 5-30 $\text{M}\Omega$, monitored throughout the voltage-clamp recording. Resting membrane potential was \sim -60 mV

for neurons and \sim -30 mV for HEK 293FT cells in current-clamp recording.

Photocurrents were measured with 500 ms light pulses in neurons voltage-clamped at -60 mV, and in HEK 293FT cells voltage-clamped at -30 mV. Light-induced membrane hyperpolarizations were measured with 500 ms light pulses in cells current-clamped at their resting membrane potential. Light pulses for all wavelengths except 660 nm and action spectrum characterization experiments were delivered with a DG-4 optical switch with 300 W xenon lamp (Sutter Instruments), controlled via TTL pulses generated through a Digidata signal generator. Green light was delivered with a 575 ± 25 nm bandpass filter (Chroma) and a 575 ± 7.5 nm bandpass filter (Chroma). Action spectra were taken with a Till Photonics Polychrome V, 150 W Xenon lamp, 15 nm monochromator bandwidth.

Data was analyzed using Clampfit (Molecular Devices) and MATLAB (Mathworks, Inc.)

6.7 *In vivo* rodent electrophysiology, optical stimulation, and data analysis.

Recordings were made in the cortex of headfixed awake mice 1-2 months after virus injection, using glass microelectrodes of 5-20 M Ω impedance filled with PBS, containing silver/silver-chloride wire electrodes. Signals were amplified with a Multiclamp 700B amplifier and digitized with a Digidata 1440, using pClamp software (Molecular Devices). A 50 mW yellow laser (SDL-593-050T, Shanghai Dream Laser) was coupled to a 200 micron-diameter optical fiber. The laser was controlled via TTL pulses generated through Digidata. Laser light power was measured with an 818-SL photodetector (Newport Co.). An optical fiber was attached to the recording glass electrode, with the tip of the fiber \sim 600 μ m laterally away from and \sim 500 μ m above the tip of the electrode (e.g., \sim 800 microns from the tip), and guided into the brain with a Siskiyou manipulator at a slow rate of \sim 1.5 μ m/s to minimize deformation of the cortical surface.

Data was analyzed using MATLAB (Mathworks, Inc.). Spikes were detected and sorted offline using Wave_clus (http://vis.caltech.edu/~rodri/Wave_clus/Wave_clus_home.htm). Neurons suppressed during light were identified by performing a paired t-test, for each neuron, between the baseline firing rate during the 5 second period before light onset vs. during the period of 5 second light illumination, across all trials for that neuron, thresholding at the $p < 0.05$ significance level. Instantaneous firing rate histograms were computed by averaging the instantaneous firing rate for each neuron, across all trials, with a histogram time bin of 20 ms duration. To determine the latency between light onset and the neural response, we swept a 20 ms-long sliding window through the electrophysiology data and looked for the earliest 20 ms period that deviated from baseline firing rate, as assessed by performing a paired t-test for the firing rate during each window vs. during the baseline period, across all trials for each neuron. Latency was defined as the time from light onset to the time at which firing rate was significantly different from baseline for the following 120 ms. The time for after-light suppression to recover back to baseline was calculated similarly.

6.8 *In vivo* primate electrophysiology, optical stimulation, and data analysis.

Primate virus injection and general surgical procedures were as previously described⁷⁴. One rhesus monkey (*Macaca mulatta*), 12 years of age, weighing ~15 kg, was used. All procedures were in accordance with the National Institutes of Health Guide for the care and use of Laboratory Animals and approved by the Massachusetts Institute of Technology Animal Care and Use Committee. Under isoflurane anesthesia, a titanium headpost and recording chambers were surgically affixed to the skull, and a craniotomy was opened up in the chamber on the parietal region. Lentivirus was injected at a rate of 0.1-0.2 ml/min at multiple depths depending on the cortex geometry. The angle of the injection was stereotactically vertical.

Primate optical stimulation and electrophysiological recording. A 100 mW green laser (SDL-532-100T, Shanghai Dream Laser Co.) was coupled to a 200 micron-diameter optical fiber (FIBER-200-UV, Ocean Optics) through a homebuilt collimator setup as described⁷⁴, resulting in a fiber tip irradiance of 100-200 mW/mm². The laser was controlled via TTL pulses driven by a pulse generator (DS8000, WPI Inc.) with the timing controlled by a computer through the software package, Cortex (<http://www.cortex.salk.edu/>). Standard tungsten electrodes of 1-2 M Ω resistance (FHC, Inc.) were guided into the brain along with a fiber attached to the electrode with the tip of the fiber slight above the tip of the electrode, typically 300-500 μ m.

Data amplification, filtering and acquisition were performed with a Multichannel Acquisition Processor (MAP) system (Plexon, Inc.). Spikes sampled at 40 kHz and filtered as 250 Hz – 8 kHz were semi-automatically detected using an interactively-set threshold, and the spike waveforms were offline sorted using principal component analysis (PCA) (Offline Sorter, Plexon, Inc.). Most of the neurons recorded had broad spike waveforms with trough-to-peak duration >200 μ s (6 out of 45 single neurons had trough-to-peak waveform durations of 100-200 μ s, suggestive of non-excitatory neurons), indicating that most of the recorded neurons (39/45) were putative excitatory neurons (Mitchell et al., 2007). Spike timing was defined as the moment of threshold crossing. During the experiment, one fiber and one electrode were lowered into the brain of an awake headfixed monkey, and optical stimulation was performed while units were recorded. During the recording period, the monkeys were awake and freely viewing, in a dimly

lit room. Occasional juice rewards were delivered to insure alertness, but no tasks nor reward contingencies were scheduled in recording sessions.

6.9 Histology

Infected HEK cells and neurons in culture were fixed in 4% paraformaldehyde and mounted in Vectashield Mounting Media (Vector Labs). Mice were perfused through the left cardiac ventricle with 4% paraformaldehyde in PBS. The brain was removed and sectioned into 40-150 um coronal sections on a cryostat. Brain sections were mounted with Vectashield HardSet (Vector Labs). Slides were visualized and imaged with a Leica DMI6000 B inverted microscope using 10x, 20x, and 40x objective lenses, and a Zeiss LSM 510 confocal microscope using 20x and 63x objective lenses.

7. Acknowledgements

First and foremost, I'd like to thank my family for the unconditional love and support they've given me over the years in everything I do, even when that meant breeding flies in the garage and ruining all the shampoo in the house.

This project would not be possible without the help and support of a huge number of people in the Synthetic Neurobiology group at MIT. In particular, I'd like to thank Ed Boyden for inspiring me to work in neuroscience, providing much-needed guidance, intellectual stimulation, and support for my work, and being an all-around great advisor. Chris Kaiser and Hugh Herr read this thesis and gave much experimental insight.

Xue Han and Brian Chow have provided invaluable perspective and suggestions about molecular biology and electrophysiology since I first joined the group as a UROP. Their mentorship has hugely impacted the way I think about science and being a scientist.

Nathan Klapoetke provided much neuron culture and experimental advice over the past two years, and always patiently answers my questions about things I don't understand.

Joe Haldeman and Sherry Turkle went out of their way to help with the not-so-scientific side of things, and helped rein in my gratuitous abuse of em dashes, ellipsis, and the second person.

I owe more than I can say to C., who never fails to brighten my day and is always there to listen, advise and encourage, and to S., who's unfailingly patient through all the revisions and angst (and revision angst), and will always be my first and last beta. They're the best friends a girl could have.

8. References

1. Boyden, E. S.; Zhang, F.; Bamberg, E.; Nagel, G.; Deisseroth, K., Millisecond-timescale, genetically targeted optical control of neural activity. *Nature Neuroscience* **2005**, *8* (9), 1263-1268.
2. Han, X.; Boyden, E. S., Multiple-color optical activation, silencing, and desynchronization of neural activity, with single-spike temporal resolution. *PloS one* **2007**, *2* (3), e299.
3. Zhang, F.; Wang, L.-P.; Brauner, M.; Liewald, J. F.; Kay, K.; Watzke, N.; Wood, P. G.; Bamberg, E.; Nagel, G.; Gottschalk, A.; Deisseroth, K., Multimodal fast optical interrogation of neural circuitry. *Nature* **2007**, *446* (7136), 633-639.
4. Lin, D.; Boyle, M. P.; Dollar, P.; Lee, H.; Lein, E. S.; Perona, P.; Anderson, D. J., Functional identification of an aggression locus in the mouse hypothalamus. *Nature* **2011**, *470* (7333), 221-226.
5. Tye, K. M.; Prakash, R.; Kim, S.-Y.; Fenno, L. E.; Grosenick, L.; Zarabi, H.; Thompson, K. R.; Gradinaru, V.; Ramakrishnan, C.; Deisseroth, K., Amygdala circuitry mediating reversible and bidirectional control of anxiety. *Nature* **2011**, *471* (7338), 358-362.
6. Cardin, J. A.; Carlén, M.; Meletis, K.; Knoblich, U.; Zhang, F.; Deisseroth, K.; Tsai, L.-H.; Moore, C. I., Driving fast-spiking cells induces gamma rhythm and controls sensory responses. *Nature* **2009**, *459* (7247), 663-667.
7. Sohal, V. S.; Zhang, F.; Yizhar, O.; Deisseroth, K., Parvalbumin neurons and gamma rhythms enhance cortical circuit performance. *Nature* **2009**, *459* (7247), 698-702.
8. Llewellyn, M. E.; Thompson, K. R.; Deisseroth, K.; Delp, S. L., Orderly recruitment of motor units under optical control in vivo. *Nature medicine* **2010**, *16* (10), 1161-1165.
9. Bruegmann, T.; Malan, D.; Hesse, M.; Beiert, T.; Fuegemann, C. J.; Fleischmann, B. K.; Sasse, P., Optogenetic control of heart muscle in vitro and in vivo. *Nature Methods* **2010**.
10. Molleman, A., Patch Clamping. *an introductory guide to patch clamp electrophysiology* **2003**, 175.
11. Hamill, O. P.; Marty, A.; Neher, E.; Sakmann, B.; Sigworth, F. J., Improved patch-clamp techniques for high-resolution current recording from cells and cell-free membrane patches. *Pflügers Archiv : European journal of physiology* **1981**, *391* (2), 85-100.
12. Spudich, J. L.; Yang, C. S.; Jung, K. H.; Spudich, E. N., Retinylidene proteins: structures and functions from archaea to humans. *Annual review of cell and developmental biology* **2000**, *16*, 365-392.

13. Sharma, A. K.; Spudich, J. L.; Doolittle, W. F., Microbial rhodopsins: functional versatility and genetic mobility. *Trends in microbiology* **2006**, *14* (11), 463-469.
14. Oesterhelt, D.; Stoeckenius, W., Rhodopsin-like protein from the purple membrane of *Halobacterium halobium*. *Nature: New biology* **1971**, *233* (39), 149-152.
15. Oesterhelt, D.; Stoeckenius, W., Functions of a new photoreceptor membrane. *Proceedings of the National Academy of Sciences of the United States of America* **1973**, *70* (10), 2853-2857.
16. Lanyi, J. K.; Weber, H. J., Spectrophotometric identification of the pigment associated with light-driven primary sodium translocation in *Halobacterium halobium*. *The Journal of biological chemistry* **1980**, *255* (1), 243-250.
17. Lanyi, J. K.; Oesterhelt, D., Identification of the retinal-binding protein in halorhodopsin. *The Journal of biological chemistry* **1982**, *257* (5), 2674-2677.
18. Schobert, B.; Lanyi, J. K., Halorhodopsin is a light-driven chloride pump. *The Journal of biological chemistry* **1982**, *257* (17), 10306-10313.
19. Hildebrand, E.; Dencher, N., Two photosystems controlling behavioural responses of *Halobacterium halobium*. *Nature* **1975**, *257* (5521), 46-48.
20. Bogomolni, R. A.; Spudich, J. L., Identification of a third rhodopsin-like pigment in phototactic *Halobacterium halobium*. *Proceedings of the National Academy of Sciences of the United States of America* **1982**, *79* (20), 6250-6254.
21. Tsuda, M., Spectral changes in the photolysis of invertebrate rhodopsin by rapid scan spectrophotometry. *Methods in enzymology* **1982**, *81*, 392-399.
22. Spudich, J. L.; Bogomolni, R. A., Mechanism of colour discrimination by a bacterial sensory rhodopsin. *Nature* **1984**, *312* (5994), 509-513.
23. Takahashi, T.; Watanabe, M.; Kamo, N.; Kobatake, Y., Negative phototaxis from blue light and the role of third rhodopsinlike pigment in *halobacterium cutirubrum*. *Biophysical Journal* **1985**, *48* (2), 235-240.
24. Spudich, E. N.; Sundberg, S. A.; Manor, D.; Spudich, J. L., Properties of a second sensory receptor protein in *Halobacterium halobium* phototaxis. *Proteins* **1986**, *1* (3), 239-246.
25. Tomioka, H.; Takahashi, T.; Kamo, N.; Kobatake, Y., Flash spectrophotometric identification of a fourth rhodopsin-like pigment in *Halobacterium halobium*. *Biochemical and biophysical research communications* **1986**, *139* (2), 389-395.
26. Marwan, W.; Oesterhelt, D., Signal formation in the halobacterial photophobic response mediated by a fourth retinal protein (P480). *Journal of molecular biology* **1987**, *195* (2), 333-342.

27. Spudich, J. L.; Bogomolni, R. A., Sensory rhodopsins of halobacteria. *Annual review of biophysics and biophysical chemistry* **1988**, *17*, 193-215.
28. Wolff, E. K.; Bogomolni, R. A.; Scherrer, P.; Hess, B.; Stoeckenius, W., Color discrimination in halobacteria: spectroscopic characterization of a second sensory receptor covering the blue-green region of the spectrum. *Proceedings of the National Academy of Sciences of the United States of America* **1986**, *83* (19), 7272-7276.
29. Kouyama, T.; Kanada, S.; Takeguchi, Y.; Narusawa, A.; Murakami, M.; Ihara, K., Crystal structure of the light-driven chloride pump halorhodopsin from *Natronomonas pharaonis*. *Journal of molecular biology* **2010**, *396* (3), 564-579.
30. Henderson, R.; Unwin, P. N., Three-dimensional model of purple membrane obtained by electron microscopy. *Nature* **1975**, *257* (5521), 28-32.
31. Grigorieff, N.; Ceska, T. A.; Downing, K. H.; Baldwin, J. M.; Henderson, R., Electron-crystallographic refinement of the structure of bacteriorhodopsin. *Journal of molecular biology* **1996**, *259* (3), 393-421.
32. Kimura, Y.; Vassilyev, D. G.; Miyazawa, A.; Kidera, A.; Matsushima, M.; Mitsuoka, K.; Murata, K.; Hirai, T.; Fujiyoshi, Y., Surface of bacteriorhodopsin revealed by high-resolution electron crystallography. *Nature* **1997**, *389* (6647), 206-211.
33. Pebay-Peyroula, E.; Rummel, G.; Rosenbusch, J. P.; Landau, E. M., X-ray structure of bacteriorhodopsin at 2.5 angstroms from microcrystals grown in lipidic cubic phases. *Science (New York, NY)* **1997**, *277* (5332), 1676-1681.
34. Luecke, H.; Richter, H. T.; Lanyi, J. K., Proton transfer pathways in bacteriorhodopsin at 2.3 angstrom resolution. *Science (New York, NY)* **1998**, *280* (5371), 1934-1937.
35. Essen, L.; Siegert, R.; Lehmann, W. D.; Oesterhelt, D., Lipid patches in membrane protein oligomers: crystal structure of the bacteriorhodopsin-lipid complex. *Proceedings of the National Academy of Sciences of the United States of America* **1998**, *95* (20), 11673-11678.
36. Luecke, H.; Schobert, B.; Richter, H. T.; Cartailler, J. P.; Lanyi, J. K., Structure of bacteriorhodopsin at 1.55 Å resolution. *Journal of molecular biology* **1999**, *291* (4), 899-911.
37. Kolbe, M.; Besir, H.; Essen, L. O.; Oesterhelt, D., Structure of the light-driven chloride pump halorhodopsin at 1.8 Å resolution. *Science (New York, NY)* **2000**, *288* (5470), 1390-1396.
38. Kunji, E. R.; von Gronau, S.; Oesterhelt, D.; Henderson, R., The three-dimensional structure of halorhodopsin to 5 Å by electron crystallography: A new unbending procedure for two-dimensional crystals by using a global reference structure. *Proceedings of the National Academy of Sciences of the United States of America* **2000**, *97* (9), 4637-4642.
39. Kunji, E. R.; Spudich, E. N.; Grishammer, R.; Henderson, R.; Spudich, J. L., Electron crystallographic analysis of two-dimensional crystals of sensory rhodopsin II: a 6.9 Å projection structure. *Journal of molecular biology* **2001**, *308* (2), 279-293.

40. Chow, B. Y.; Han, X.; Dobry, A. S.; Qian, X.; Chuong, A.; Li, M.; Henninger, M. A.; Belfort, G. M.; Lin, Y.; Monahan, P. E.; Boyden, E. S., High-performance genetically targetable optical neural silencing by light-driven proton pumps. *Nature* **2010**, *463* (7277), 98-102.
41. Han, X.; Qian, X.; Stern, P.; Chuong, A.; Boyden, E. S., Informational lesions: optical perturbation of spike timing and neural synchrony via microbial opsin gene fusions. *Frontiers in molecular neuroscience* **2009**, *2*, 12.
42. Zhao, S.; Cunha, C.; Zhang, F.; Liu, Q.; Gloss, B.; Deisseroth, K.; Augustine, G. J.; Feng, G., Improved expression of halorhodopsin for light-induced silencing of neuronal activity. *Brain cell biology* **2008**, *36* (1-4), 141-154.
43. Rüdiger, M.; Haupts, U.; Gerwert, K.; Oesterhelt, D., Chemical reconstitution of a chloride pump inactivated by a single point mutation. *The EMBO journal* **1995**, *14* (8), 1599-1606.
44. Rüdiger, M.; Oesterhelt, D., Specific arginine and threonine residues control anion binding and transport in the light-driven chloride pump halorhodopsin. *The EMBO journal* **1997**, *16* (13), 3813-3821.
45. Sato, M.; Kikukawa, T.; Araiso, T.; Okita, H.; Shimono, K.; Kamo, N.; Demura, M.; Nitta, K., Ser-130 of Natronobacterium pharaonis halorhodopsin is important for the chloride binding. *Biophysical chemistry* **2003**, *104* (1), 209-216.
46. Sato, M.; Kikukawa, T.; Araiso, T.; Okita, H.; Shimono, K.; Kamo, N.; Demura, M.; Nitta, K., Roles of Ser130 and Thr126 in chloride binding and photocycle of pharaonis halorhodopsin. *Journal of biochemistry* **2003**, *134* (1), 151-158.
47. Mogi, T.; Stern, L. J.; Chao, B. H.; Khorana, H. G., Structure-function studies on bacteriorhodopsin. VIII. Substitutions of the membrane-embedded prolines 50, 91, and 186: the effects are determined by the substituting amino acids. *The Journal of biological chemistry* **1989**, *264* (24), 14192-14196.
48. Mogi, T.; Marti, T.; Khorana, H. G., Structure-function studies on bacteriorhodopsin. IX. Substitutions of tryptophan residues affect protein-retinal interactions in bacteriorhodopsin. *The Journal of biological chemistry* **1989**, *264* (24), 14197-14201.
49. Mogi, T.; Stern, L. J.; Hackett, N. R.; Khorana, H. G., Bacteriorhodopsin mutants containing single tyrosine to phenylalanine substitutions are all active in proton translocation. *Proceedings of the National Academy of Sciences of the United States of America* **1987**, *84* (16), 5595-5599.
50. Mogi, T.; Stern, L. J.; Marti, T.; Chao, B. H.; Khorana, H. G., Aspartic acid substitutions affect proton translocation by bacteriorhodopsin. *Proceedings of the National Academy of Sciences of the United States of America* **1988**, *85* (12), 4148-4152.

51. Greenhalgh, D. A.; Farrens, D. L.; Subramaniam, S.; Khorana, H. G., Hydrophobic amino acids in the retinal-binding pocket of bacteriorhodopsin. *The Journal of biological chemistry* **1993**, *268* (27), 20305-20311.
52. Muñoz-Jordán, J. L.; Laurent-Rolle, M.; Ashour, J.; Martínez-Sobrido, L.; Ashok, M.; Lipkin, W. I.; García-Sastre, A., Inhibition of alpha/beta interferon signaling by the NS4B protein of flaviviruses. *Journal of virology* **2005**, *79* (13), 8004-8013.
53. Jungnickel, B.; Rapoport, T. A., A posttargeting signal sequence recognition event in the endoplasmic reticulum membrane. *Cell* **1995**, *82* (2), 261-270.
54. Gradinaru, V.; Thompson, K. R.; Deisseroth, K., eNpHR: a *Natronomonas halorhodopsin* enhanced for optogenetic applications. *Brain cell biology* **2008**, *36* (1-4), 129-139.
55. Váró, G., Analogies between halorhodopsin and bacteriorhodopsin. *Biochimica et Biophysica Acta (BBA)-Bioenergetics* **2000**.
56. Mukohata, Y.; Ihara, K.; Tamura, T.; Sugiyama, Y., Halobacterial rhodopsins. *Journal of biochemistry* **1999**, *125* (4), 649-657.
57. Soppa, J.; Duschl, J.; Oesterhelt, D., Bacterioopsin, haloopsin, and sensory opsin I of the halobacterial isolate *Halobacterium* sp. strain SG1: three new members of a growing family. *Journal of bacteriology* **1993**, *175* (9), 2720-2726.
58. Kitajima, T.; Hirayama, J.; Ihara, K.; Sugiyama, Y.; Kamo, N.; Mukohata, Y., Novel bacterial rhodopsins from *Haloarcula vallismortis*. *Biochemical and biophysical research communications* **1996**, *220* (2), 341-345.
59. Klare, J. P.; Chizhov, I.; Engelhard, M., Microbial rhodopsins: scaffolds for ion pumps, channels, and sensors. *Results and problems in cell differentiation* **2008**, *45*, 73-122.
60. Baliga, N. S.; Bonneau, R.; Facciotti, M. T.; Pan, M.; Glusman, G.; Deutsch, E. W.; Shannon, P.; Chiu, Y.; Weng, R. S.; Gan, R. R.; Hung, P.; Date, S. V.; Marcotte, E.; Hood, L.; Ng, W. V., Genome sequence of *Haloarcula marismortui*: a halophilic archaeon from the Dead Sea. *Genome research* **2004**, *14* (11), 2221-2234.
61. Bolhuis, H.; Palm, P.; Wende, A.; Falb, M.; Rampp, M.; Rodriguez-Valera, F.; Pfeiffer, F.; Oesterhelt, D., The genome of the square archaeon *Haloquadratum walsbyi*: life at the limits of water activity. *BMC genomics* **2006**, *7*, 169.
62. Mongodin, E. F.; Nelson, K. E.; Daugherty, S.; Deboy, R. T.; Wister, J.; Khouri, H.; Weidman, J.; Walsh, D. A.; Papke, R. T.; Sanchez Perez, G.; Sharma, A. K.; Nesbø, C. L.; MacLeod, D.; Baptiste, E.; Doolittle, W. F.; Charlebois, R. L.; Legault, B.; Rodriguez-Valera, F., The genome of *Salinibacter ruber*: convergence and gene exchange among hyperhalophilic bacteria and archaea. *Proceedings of the National Academy of Sciences of the United States of America* **2005**, *102* (50), 18147-18152.

63. Gunde-Cimerman, N.; Oren, A.; Plemenitaš, A., *Adaptation to life at high salt concentrations in Archaea, Bacteria, and Eukarya*. Kluwer Academic Pub: 2005; p 576.
64. Espagne, E.; Lespinet, O.; Malagnac, F.; Da Silva, C.; Jaillon, O.; Porcel, B. M.; Couloux, A.; Aury, J.-M.; Ségurens, B.; Poulain, J.; Anthouard, V.; Grossetete, S.; Khalili, H.; Coppin, E.; Déquard-Chablat, M.; Picard, M.; Contamine, V.; Arnaise, S.; Bourdais, A.; Berteaux-Lecellier, V.; Gautheret, D.; de Vries, R. P.; Battaglia, E.; Coutinho, P. M.; Danchin, E. G.; Henrissat, B.; Khoury, R. E.; Sainsard-Chanet, A.; Boivin, A.; Pinan-Lucarré, B.; Sellem, C. H.; Debuchy, R.; Wincker, P.; Weissenbach, J.; Silar, P., The genome sequence of the model ascomycete fungus *Podospira anserina*. *Genome biology* **2008**, *9* (5), R77.
65. Bieszke, J. A.; Braun, E. L.; Bean, L. E.; Kang, S.; Natvig, D. O.; Borkovich, K. A., The *nop-1* gene of *Neurospora crassa* encodes a seven transmembrane helix retinal-binding protein homologous to archaeal rhodopsins. *Proceedings of the National Academy of Sciences of the United States of America* **1999**, *96* (14), 8034-8039.
66. Waschuk, S. A.; Bezerra, A. G.; Shi, L.; Brown, L. S., Leptosphaeria rhodopsin: bacteriorhodopsin-like proton pump from a eukaryote. *Proceedings of the National Academy of Sciences of the United States of America* **2005**, *102* (19), 6879-6883.
67. Tateno, M.; Ihara, K.; Mukohata, Y., The novel ion pump rhodopsins from *Haloarcula* form a family independent from both the bacteriorhodopsin and archaerhodopsin families/tribes. *Archives of biochemistry and biophysics* **1994**, *315* (1), 127-132.
68. Béjà, O.; Aravind, L.; Koonin, E. V.; Suzuki, M. T.; Hadd, A.; Nguyen, L. P.; Jovanovich, S. B.; Gates, C. M.; Feldman, R. A.; Spudich, J. L.; Spudich, E. N.; DeLong, E. F., Bacterial rhodopsin: evidence for a new type of phototrophy in the sea. *Science (New York, NY)* **2000**, *289* (5486), 1902-1906.
69. Wang, W.-W.; Sineshchekov, O. A.; Spudich, E. N.; Spudich, J. L., Spectroscopic and photochemical characterization of a deep ocean proteorhodopsin. *The Journal of biological chemistry* **2003**, *278* (36), 33985-33991.
70. Tsunoda, S. P.; Ewers, D.; Gazzarrini, S.; Moroni, A.; Gradmann, D.; Hegemann, P., H⁺-pumping rhodopsin from the marine alga *Acetabularia*. *Biophysical Journal* **2006**, *91* (4), 1471-1479.
71. Ihara, K.; Umemura, T.; Katagiri, I.; Kitajima-Ihara, T.; Sugiyama, Y.; Kimura, Y.; Mukohata, Y., Evolution of the archaeal rhodopsins: evolution rate changes by gene duplication and functional differentiation. *Journal of molecular biology* **1999**, *285* (1), 163-174.
72. Han, X.; Chow, B. Y.; Huihui, Z.; Klapoetke, N. C.; Chuong, A.; Rajimehr, R.; Yang, A.; Baratta, M. V.; Winkle, J.; Desimone, R.; Boyden, E. S., A High-Light Sensitivity Optical Neural Silencer: Development and Application to Optogenetic Control of Non-Human Primate Cortex. *Frontiers in Systems Neuroscience* **2011**, *5*.

73. Thompson, J. D.; Higgins, D. G.; Gibson, T. J., CLUSTAL W: improving the sensitivity of progressive multiple sequence alignment through sequence weighting, position-specific gap penalties and weight matrix choice. *Nucleic acids research* **1994**, *22* (22), 4673-4680.
74. Han, X.; Qian, X.; Bernstein, J. G.; Zhou, H.-h.; Franzesi, G. T.; Stern, P.; Bronson, R. T.; Graybiel, A. M.; Desimone, R.; Boyden, E. S., Millisecond-timescale optical control of neural dynamics in the nonhuman primate brain. *Neuron* **2009**, *62* (2), 191-198.
75. Mitchell, J. F.; Sundberg, K. A.; Reynolds, J. H., Differential attention-dependent response modulation across cell classes in macaque visual area V4. *Neuron* **2007**, *55* (1), 131-141.
76. Chow, B. Y.; Chuong, A.; Klapoetke, N. C.; Boyden, E. S., Synthetic physiology strategies for adapting tools from nature for genetically targeted control of fast biological processes. *Methods in enzymology* **2011**, *497*, 425-443.
77. Richardson, S. M.; Nunley, P. W.; Yarrington, R. M.; Boeke, J. D.; Bader, J. S., GeneDesign 3.0 is an updated synthetic biology toolkit. *Nucleic acids research* **2010**, *38* (8), 2603-2606.
78. Welch, M.; Govindarajan, S.; Ness, J. E.; Villalobos, A.; Gurney, A.; Minshull, J.; Gustafsson, C., Design parameters to control synthetic gene expression in *Escherichia coli*. *PLoS one* **2009**, *4* (9), e7002.
79. Wu, G.; Bashir-Bello, N.; Freeland, S. J., The Synthetic Gene Designer: a flexible web platform to explore sequence manipulation for heterologous expression. *Protein expression and purification* **2006**, *47* (2), 441-445.
80. Enami, N.; Yoshimura, K.; Murakami, M.; Okumura, H.; Ihara, K.; Kouyama, T., Crystal structures of archaerhodopsin-1 and -2: Common structural motif in archaeal light-driven proton pumps. *Journal of molecular biology* **2006**, *358* (3), 675-685.
81. Luecke, H.; Schobert, B.; Richter, H. T.; Cartailler, J. P.; Lanyi, J. K., Structural changes in bacteriorhodopsin during ion transport at 2 angstrom resolution. *Science (New York, NY)* **1999**, *286* (5438), 255-261.
82. Luecke, H.; Schobert, B.; Lanyi, J. K.; Spudich, E. N.; Spudich, J. L., Crystal structure of sensory rhodopsin II at 2.4 angstroms: insights into color tuning and transducer interaction. *Science (New York, NY)* **2001**, *293* (5534), 1499-1503.
83. Yoshimura, K.; Kouyama, T., Structural role of bacterioruberin in the trimeric structure of archaerhodopsin-2. *Journal of molecular biology* **2008**, *375* (5), 1267-1281.
84. Hackett, N. R.; Stern, L. J.; Chao, B. H.; Kronis, K. A.; Khorana, H. G., Structure-function studies on bacteriorhodopsin. V. Effects of amino acid substitutions in the putative helix F. *The Journal of biological chemistry* **1987**, *262* (19), 9277-9284.

85. Marinetti, T.; Subramaniam, S.; Mogi, T.; Marti, T.; Khorana, H. G., Replacement of aspartic residues 85, 96, 115, or 212 affects the quantum yield and kinetics of proton release and uptake by bacteriorhodopsin. *Proceedings of the National Academy of Sciences of the United States of America* **1989**, *86* (2), 529-533.
86. Otto, H.; Marti, T.; Holz, M.; Mogi, T.; Lindau, M.; Khorana, H. G.; Heyn, M. P., Aspartic acid-96 is the internal proton donor in the reprotonation of the Schiff base of bacteriorhodopsin. *Proceedings of the National Academy of Sciences of the United States of America* **1989**, *86* (23), 9228-9232.
87. Stern, L. J.; Khorana, H. G., Structure-function studies on bacteriorhodopsin. X. Individual substitutions of arginine residues by glutamine affect chromophore formation, photocycle, and proton translocation. *The Journal of biological chemistry* **1989**, *264* (24), 14202-14208.
88. Gilles-Gonzalez, M. A.; Engelman, D. M.; Khorana, H. G., Structure-function studies of bacteriorhodopsin XV. Effects of deletions in loops B-C and E-F on bacteriorhodopsin chromophore and structure. *The Journal of biological chemistry* **1991**, *266* (13), 8545-8550.
89. Marti, T.; Otto, H.; Mogi, T.; Rösselet, S. J.; Heyn, M. P.; Khorana, H. G., Bacteriorhodopsin mutants containing single substitutions of serine or threonine residues are all active in proton translocation. *The Journal of biological chemistry* **1991**, *266* (11), 6919-6927.
90. Subramaniam, S.; Greenhalgh, D. A.; Khorana, H. G., Aspartic acid 85 in bacteriorhodopsin functions both as proton acceptor and negative counterion to the Schiff base. *The Journal of biological chemistry* **1992**, *267* (36), 25730-25733.
91. Berndt, A.; Yizhar, O.; Gunaydin, L. A.; Hegemann, P.; Deisseroth, K. *Bi-stable neural state switches.*; Mar, 2009; pp 229-234.
92. Lin, J. Y.; Lin, M. Z.; Steinbach, P.; Tsien, R. Y., Characterization of engineered channelrhodopsin variants with improved properties and kinetics. *Biophysical Journal* **2009**, *96* (5), 1803-1814.
93. Wang, H.; Sugiyama, Y.; Hikima, T.; Sugano, E.; Tomita, H.; Takahashi, T.; Ishizuka, T.; Yawo, H., Molecular determinants differentiating photocurrent properties of two channelrhodopsins from *Chlamydomonas*. *The Journal of biological chemistry* **2009**, *284* (9), 5685-5696.
94. Gunaydin, L. A.; Yizhar, O.; Berndt, A.; Sohal, V. S.; Deisseroth, K.; Hegemann, P., Ultrafast optogenetic control. *Nature Neuroscience* **2010**, *13* (3), 387-392.
95. Gradinaru, V.; Zhang, F.; Ramakrishnan, C.; Mattis, J.; Prakash, R.; Diester, I.; Goshen, I.; Thompson, K. R.; Deisseroth, K., Molecular and cellular approaches for diversifying and extending optogenetics. *Cell* **2010**, *141* (1), 154-165.

96. Weber, K.; Bartsch, U.; Stocking, C.; Fehse, B., A multicolor panel of novel lentiviral "gene ontology" (LeGO) vectors for functional gene analysis. *Molecular therapy : the journal of the American Society of Gene Therapy* **2008**, *16* (4), 698-706.
97. Mizuguchi, H.; Xu, Z.; Ishii-Watabe, A.; Uchida, E.; Hayakawa, T., IRES-dependent second gene expression is significantly lower than cap-dependent first gene expression in a bicistronic vector. *Molecular therapy : the journal of the American Society of Gene Therapy* **2000**, *1* (4), 376-382.
98. Hennecke, M.; Kwissa, M.; Metzger, K.; Oumard, A.; Kröger, A.; Schirmbeck, R.; Reimann, J.; Hauser, H., Composition and arrangement of genes define the strength of IRES-driven translation in bicistronic mRNAs. *Nucleic acids research* **2001**, *29* (16), 3327-3334.
99. Yu, X.; Zhan, X.; D'Costa, J.; Tanavde, V. M.; Ye, Z.; Peng, T.; Malehorn, M. T.; Yang, X.; Civin, C. I.; Cheng, L., Lentiviral vectors with two independent internal promoters transfer high-level expression of multiple transgenes to human hematopoietic stem-progenitor cells. *Molecular therapy : the journal of the American Society of Gene Therapy* **2003**, *7* (6), 827-838.
100. Osti, D.; Marras, E.; Ceriani, I.; Grassini, G., Comparative analysis of molecular strategies attenuating positional effects in lentiviral vectors carrying multiple genes. *Journal of virological ...* **2006**.
101. Tang, W.; Ehrlich, I.; Wolff, S. B. E.; Michalski, A.-M.; Wölfl, S.; Hasan, M. T.; Lüthi, A.; Sprengel, R., Faithful expression of multiple proteins via 2A-peptide self-processing: a versatile and reliable method for manipulating brain circuits. *The Journal of neuroscience : the official journal of the Society for Neuroscience* **2009**, *29* (27), 8621-8629.
102. Ma, D., Role of ER Export Signals in Controlling Surface Potassium Channel Numbers. *Science (New York, NY)* **2001**, *291* (5502), 316-319.
103. Stockklausner, C.; Klöcker, N., Surface expression of inward rectifier potassium channels is controlled by selective Golgi export. *The Journal of biological chemistry* **2003**, *278* (19), 17000-17005.
104. Hofherr, A.; Fakler, B.; Klöcker, N., Selective Golgi export of Kir2.1 controls the stoichiometry of functional Kir2.x channel heteromers. *Journal of cell science* **2005**, *118* (Pt 9), 1935-1943.
105. Dunn, R. J.; Hackett, N. R.; McCoy, J. M.; Chao, B. H.; Kimura, K.; Khorana, H. G., Structure-function studies on bacteriorhodopsin. I. Expression of the bacterio-opsin gene in *Escherichia coli*. *J Biol Chem* **1987**, *262* (19), 9246-54.
106. Nagel, G.; Szellas, T.; Huhn, W.; Kateriya, S.; Adeishvili, N.; Berthold, P.; Ollig, D.; Hegemann, P.; Bamberg, E., Channelrhodopsin-2, a directly light-gated cation-selective membrane channel. *Proceedings of the National Academy of Sciences of the United States of America* **2003**, *100* (24), 13940-13945.

107. Li, X.; Gutierrez, D. V.; Hanson, M. G.; Han, J.; Mark, M. D.; Chiel, H.; Hegemann, P.; Landmesser, L. T.; Herlitze, S., Fast noninvasive activation and inhibition of neural and network activity by vertebrate rhodopsin and green algae channelrhodopsin. *Proceedings of the National Academy of Sciences of the United States of America* **2005**, *102* (49), 17816-17821.
108. Albeanu, D. F.; Soucy, E.; Sato, T. F.; Meister, M.; Murthy, V. N., LED arrays as cost effective and efficient light sources for widefield microscopy. *PloS one* **2008**, *3* (5), e2146.
109. Prigge, M.; Rösler, A.; Hegemann, P., Fast, repetitive light-activation of CaV3.2 using channelrhodopsin 2. *Channels (Austin, Tex.)* **2010**, *4* (3), 241-247.
110. Dunlop, J.; Bowlby, M.; Peri, R.; Vasilyev, D.; Arias, R., High-throughput electrophysiology: an emerging paradigm for ion-channel screening and physiology. *Nature reviews. Drug discovery* **2008**, *7* (4), 358-368.
111. Berthold, P.; Tsunoda, S. P.; Ernst, O. P.; Mages, W.; Gradmann, D.; Hegemann, P., Channelrhodopsin-1 initiates phototaxis and photophobic responses in chlamydomonas by immediate light-induced depolarization. *The Plant cell* **2008**, *20* (6), 1665-1677.